

Physical modeling of viscous disc evolution around magnetized neutron star. Aql X-1 2013 outburst decay

Galina Lipunova,^{1*} Konstantin Malanchev,^{1,2} Sergey Tsygankov,^{3,4} Nikolai Shakura,^{1,5}
 Andrei Tavleev,^{6,1} Dmitry Kolesnikov¹

¹*Moscow Lomonosov State University Sternberg Astronomical Institute, Moscow 119992, Universitetskii pr., 13, Russia*

²*Department of Astronomy, University of Illinois at Urbana-Champaign, 1002 West Green Street, Urbana, IL 61801, USA*

³*Department of Physics and Astronomy, FI-20014 University of Turku, Finland*

⁴*Space Research Institute of the Russian Academy of Sciences, Profsoyuznaya Str. 84/32, Moscow 117997, Russia*

⁵*Kazan Federal University, 420008 Kazan, Russia*

⁶*Physics Faculty of Moscow Lomonosov State University, Moscow 119992, Russia*

Accepted 2021 November 10. Received 2021 November 10; in original form 2021 March 5

ABSTRACT

We present a model of a viscously evolving accretion disc around a magnetized neutron star. The model features the varying outer radius of the hot ionized part of the disc due to cooling and the varying inner radius of the disc due to interaction with the magnetosphere. It also includes hindering of accretion on the neutron star because of the centrifugal barrier and irradiation of the outer disc and companion star by X-rays from the neutron star and disc. When setting inner boundary conditions, we take into account that processes at the inner disc occur on a time scale much less than the viscous time scale of the whole disc. We consider three types of outflow from the disc inner edge: zero outflow, one based on MHD calculations, and a very efficient propeller mechanism. The light curves of an X-ray transient after the outburst peak can be calculated by a corresponding, publicly available code. We compare observed light curves of the 2013 burst of Aql X-1 in X-ray and optical bands with modeled ones. We find that the fast drop of the 0.3 – 10 keV flux can be solely explained by a radial shrinking of the hot disc. At the same time, models with the neutron star magnetic field $> 10^8$ G have better fits because the accretion efficiency behaviour emphasizes the ‘knee’ on the light curve. We also find that a plato emission can be produced by a disc-reservoir with stalled accretion.

Key words: accretion, accretion discs – stars:neutron – binaries: close – stars: individual: Aql X-1

1 INTRODUCTION

Brightest transient phenomena in X-ray binary systems are closely connected to long-term dynamical evolution of viscous accretion discs around compact objects. A change of the mass accretion rate on a compact object, which is observed as an outburst lasting many days, can be induced by an instability in a disc or a rise of mass income from a companion star. In low-mass X-ray binaries (LMXBs), for instance, the neighbour star fills its Roche lobe and leaks slowly into the disc until an outburst occurs. The thermal–viscous disc instability (see, e.g., Hameury 2020, and references therein) is now generally thought to be the basic cause of outbursts of dwarf novae and low-mass X-ray binaries (LMXBs). According to this model, ionization wave goes through a substantial part of a disc before a burst reaches its peak. The temperature and viscosity coefficient in the ionized zone rise. Near the peak the size of the ionized hot zone is the largest and the disc radial structure can be described by a quasi-stationary, standard α -disc.

Viscous evolution of an accretion disc can be described by a single equation, which follows from equations of the mass and angular momentum conservation. This is true when assumptions underly-

ing the standard disc model (Shakura & Sunyaev 1973) hold: a disc is geometrically thin and optically thick and the local energy balance works. The standard disc model is widely and successfully used to interpret observations and to describe disc physics. Plugged into the viscous evolution equation, the standard disc with constant outer radius produces a fast-rise quasi-exponential-decay (FRED) light curve (Lipunova & Shakura 2000; Lipunova 2015). However, FRED light curves are rather exceptional cases. Observed irregularities, plateaus, breaks, and reflares of the light curves demonstrate physical complexity calling for further analytic and numerical considerations (see, e.g., Bagińska et al. 2021).

Comparing discs around neutrons stars and black holes, we bound to acknowledge that disc evolution around neutron stars is even more complicated and fascinating. The neutron stars are extreme objects and emitters of the electromagnetic radiation of various kinds (e.g., Özel & Freire 2016). Different species of sources with neutron stars are observed thanks to the various combination of the key parameters: the spin and magnetic field of the star, the density and angular momentum of surrounding matter (Lipunov 1992).

In X-ray transients, both with black holes (BHXT) and neutron stars (NSXT), neat FRED light curves are exceptional. A common feature is a change of the light curve slope during a decay to a faster one. Models, explaining such non-trivial light curves of BHXTs consist exclusively on the developments in the discs themselves. In the

* E-mail: gvlipunova@sai.msu.ru

NSXTs, the physics of the central star may have impact on the light curves. Sudden drops of X-ray flux are sometimes regarded as manifestations of the accretion rate being blocked on its way to the rotating neutron star by a sufficiently large magnetosphere (Stella et al. 1986; Cui 1997; Campana et al. 1998; Gilfanov et al. 1998; Raguzova & Lipunov 1998; Zhang et al. 1998a; Alpar 2001; Hartman et al. 2009, 2011; Asai et al. 2013; Matsuoka & Asai 2013; Campana et al. 2014; Tsygankov et al. 2016; Fürst et al. 2017; Lutovinov et al. 2017). The hindering of accretion onto a neutron star can occur if the disc is disrupted by the magnetic field beyond the corotation radius (Shvartsman 1970; Pringle & Rees 1972; Lamb et al. 1973; Davidson & Ostriker 1973), defined as the radius where the Keplerian frequency equals the star’s spin frequency. In such situation, as suggested by theoretical and numerical modelings, the matter can be expelled from the system, due to a ‘propeller effect’ (Illarionov & Sunyaev 1975), and/or remain in the disc (Sunyaev & Shakura 1977; Lipunov 1980; Spruit & Taam 1993; D’Angelo & Spruit 2010; Hartman et al. 2011; D’Angelo & Spruit 2012; Zanni & Ferreira 2013; Parfrey & Tchekhovskoy 2017; Parfrey et al. 2017; Romanova et al. 2018, hereafter R18).

On the other hand, a specific change in the disc evolution, manifested as a steepening of a light curve slope, can happen due to a critical cooling at the outer disc, which leads to a decrease of the hot disc size¹ (King & Ritter 1998; Gilfanov et al. 1998; Shahbaz et al. 1998; Powell et al. 2007; Campana et al. 2013). This is an essential component of the ‘DIM’ — a Disc Instability Model. Then, theoretically, the propeller effect is not required to explain a fast drop of the flux. A picture unifying the DIM scenario and the propeller effect was considered by Hartman et al. (2011); Güngör et al. (2014).

In the present work we take a step towards a detailed modeling of a burst in accretion discs of NSXTs. To address a complex evolution of an accretion disc around a magnetized neutron star, we have built a multi-component physical 1D radial model to calculate the disc evolution after the peak of an outburst. Up to now, numerical 3D simulations can hardly address the whole disc. This proceeds from the vast difference of scales, temporal and spatial, which need to be involved in a resource-consuming 3D model of a whole disc. The 1D studies of accretion on neutron stars also tend to focus on the innermost disc radii (Spruit & Taam 1993; D’Angelo & Spruit 2010) with an exception of the work by Armitage & Clarke (1996) who studied non-steady accretion discs around single and binary magnetized T Tauri stars.

Our model includes principal ingredients of the evolution of an accretion disc around a neutron star. We do not attempt a deep sophistication of each ingredient of our model at this stage. Instead, proper parametrizations are proposed that allow us to construct a reasonably fast numerical scheme which calculates light curves of an accreting neutron star surrounded by a viscously-evolving accretion disc. A corresponding numerical computer code² is based on a previously published FREDDI-code, which calculates the burst evolution of a BHXT (Malanchev & Lipunova 2016; Lipunova & Malanchev 2017).

We demonstrate the capacity of our code by successfully modeling an outburst of a well-studied X-ray transient – Aql X-1. In 2013, its outburst was observed by X-ray instruments, including the Neil Gehrels Swift observatory, and also by many optical ground observa-

tories. The characteristic knee on the light curve was observed around ~ 45 day from the peak. Using our numerical code, we successfully explain such evolution of flux in X-ray and optical.

We find that to explain the X-ray light curve of Aql X-1 of the 2013 burst, the size of the zone with ionized material should be decreasing. This is in agreement with the DIM model. We study if the observed light curves demonstrate any indications of the magnetosphere-disc interaction within our scheme. We also explore the possibility that the plato X-ray emission is generated by the heat released in a remnant disc with the inner edge stopped beyond the corotation radius.

In §2, we present our model. In §3, the observational data and its reduction are described. Results of modeling can be found in §4. We compare our model and its results with others, discuss low plato emission and the effect of the neutron star magnetic field and irradiation parameter’s value on the light curves in §5. We summarize in §6.

2 MODEL OF MAGNETICALLY-TRUNCATED SELF-IRRADIATED DISC DURING OUTBURST

Viscous evolution of an accretion disc around a central object of mass M_\star is described by the equation of diffusion type (see, e.g., Lyubarskij & Shakura 1987):

$$\frac{\partial \Sigma}{\partial t} = \frac{1}{4\pi} \frac{(GM_\star)^2}{h^3} \frac{\partial^2 F}{\partial h^2}, \quad (1)$$

where $h \equiv \sqrt{GM_\star r}$ is the specific angular momentum, Σ is the surface density, $F = 2\pi W_{r\varphi} r^2$ is the viscous torque related to the height-integrated viscous stress tensor. For the α -disc (Shakura 1973), the latter is expressed as

$$W_{r\varphi} = \int_{-z_0}^{+z_0} \alpha P dz, \quad (2)$$

where P is the pressure in the disc, z_0 is the semithickness.

The accretion rate in an evolving disc can be expressed as follows:

$$\dot{M} = \frac{\partial F}{\partial h}. \quad (3)$$

Equation (1) can be solved analytically in a number of cases (Lynden-Bell & Pringle 1974; Lyubarskij & Shakura 1987; Pringle 1991; Tanaka 2011; Eksi 2012; Illenseer & Duschl 2015; Lipunova 2015; Rafikov 2016; Balbus & Mummery 2018; Mush-tukov et al. 2019; Nixon & Pringle 2020). Such solutions imply uniform properties of viscosity and uniform analytic relation $F(\Sigma)$ over a disc and its fixed or freely expanding outer radius. In physically motivated models of discs, realistic constrains complicate the disc evolution calling for numerical approaches. First, the boundaries of the fast-evolving hot zone of the disc move. Second, a numerical (non-analytic) solution of the vertical structure can provide a relation between the surface density Σ and the viscous torque F .

Let us emphasize some key features demonstrated by analytic solutions for the discs with limited outer radius. It is established that the rate of the disc mass variation is determined by the *values* at the disc outer radius and the *type* of condition at the inner radius. The inner rings of the disc adjust themselves according to an inner boundary condition on the local viscous time scale, that is, significantly faster than the global viscous time scale t_{visc} . This means that in a non-stationary disc with time-dependent $\dot{M}(t)$ but a fixed inner-boundary condition, a quasi-stationary distribution of parameters, determined by the inner condition, is applicable in its inner part. If the matter

¹ Usually this change is called a ‘transition from an exponential decay to a linear one’ since such laws of $\dot{M}(t)$ are realized in the models with constant viscosity.

² available at GitHub through <http://xray.sai.msu.ru/sciwork>

freely leaves the disc at its inner edge then the accretion rate is approximately constant over radius at each moment, $\dot{M}(r) \approx \text{const}$, and the disc mass varies as $\dot{M}_{\text{disc}} \sim M_{\text{disc}}/t_{\text{visc}} \propto F_{\text{out}}/h_{\text{out}}$; if, on the contrary, the mass flow through the inner radius is blocked then a horizontal F -profile develops: $\dot{M}(r) = 0$.

If the central object is magnetized, the magnetic field can disrupt the accretion flow at the radius comparable with the Alfvén radius. Thus, the inner radius of disc depends on the accretion rate. Moreover, the inner disc can lack the axial symmetry and one has to take into account the uncertainty of a definition of the inner boundary. The instant accretion rate through the disc inner edge is determined by a complex of local MHD, thermal, and dynamical processes. The global disc evolution (or $\dot{M}_{\text{disc}}(t)$), however, depends on the inner conditions averaged over a time period comparable to the global viscous time.

The implications for a disc around a neutron star during an outburst are the following. Consider a disc with diminishing accretion rate. The inner radius is shifting away from a magnetized star, eventually reaching the corotation radius. Suppose that, when $R_{\text{in}} \gtrsim R_{\text{cor}}$, the matter is mostly trapped in the disc near the inner edge and not expelled. For example, D’Angelo & Spruit (2010) argue that this would be the case if the inner edge is close to the corotation radius. Then, on the time-scale of the viscous time at the inner radius, the matter is piling there until it pushes the magnetosphere so that the accretion on the star is possible again. The viscous time at the corotation radius in the disc with a semithickness z_0 can be estimated as $t_{\text{vis}}(R_{\text{cor}}) = t_{\text{K}}/\alpha/(z_0/r)^2 \sim P_{\star} (R_{\text{cor}}/z_0)^2/\alpha \sim (10^2 - 10^3)P_{\star}$, where $t_{\text{K}} \equiv 2\pi/\omega_{\text{K}}$ and P_{\star} is the star spin period. For a millisecond pulsar, $t_{\text{vis}}(R_{\text{cor}})$ can be $\sim 0.1 - 1$ s. Thus, on such times the matter ‘brims over’ the centrifugal barrier again and again, while there is a flow from the outer disc parts (a ‘quasi-propeller’ mode as coined by Hartman et al. 2011). Analytic descriptions of such oscillations were developed by Spruit & Taam (1993) and D’Angelo & Spruit (2010) in time-dependent radial models (hence the ‘Spruit-Taam instability’). Furthermore, Ertan (2017, 2018) studied the conditions for propelling the matter from the disc, when its edge is beyond R_{cor} , and argued that steady propelling could not happen arbitrary far from R_{cor} , thus also bringing about the billowing outflow events.

Oscillating character of the flow stopped beyond the corotation radius was also demonstrated in numerical simulations by Romanova et al. (2005); Ustyugova et al. (2006); Romanova et al. (2009); Zanni & Ferreira (2013); Lii et al. (2014); Parfrey et al. (2017), R18. In particular, R18 have shown that the inner disc radius R_{in} oscillates around some value: when R_{in} is far enough, the matter accumulates; the radius gradually decreases and provokes a spike of ejection (and sometimes accretion) associated with a magnetic-lines inflation. The accretion events are highly asymmetric relative to the vertical coordinate z and the azimuth. R18 also report that the inner radius is varying, permitting accretion, on time scales of 0.1 s when scaled to typical parameters of AXMPs. These variations cannot be seen in the outburst long-term light curves, but, presumably, they can be observed on proper time-scales.

To sum up, if one sets an effective averaging condition at the inner radius, the whole disc evolution can be calculated by solving Eq. (1). For this we use the code FREDDI (Malanchev & Lipunov 2016) developed for modeling burst light curves of BHXTs, utilizing the solution for vertical structure of a geometrically-thin disc in an analytic form (see Appendix §A). In further subsections we describe new features of the code.

2.1 Inner radius of the disc

If the accretion rate on a magnetized neutron star is high, the accretion disc can reach the star surface or spiral down to it from the radius of the last stable orbit (see, e.g., Syunyaev & Shakura 1986). Otherwise, the disc is truncated by the magnetosphere.

Models of discs threaded by magnetic lines assume that the inner radius can be found by comparing the disc-height integrated magnetic stress with the angular momentum flux, see, e.g. Wang (1996); Armitage & Clarke (1996); Matt & Pudritz (2005); Kluźniak & Rappaport (2007). For diamagnetic discs, a pressure balance is employed instead (e.g., Elsner & Lamb 1977; Syunyaev & Shakura 1977; Lipunov 1978; Aly 1980; Chashkina et al. 2017). Both approaches yield the same expression for R_{in} , within some dimensionless factor. We choose for the present work the following parametrization:

$$R_{\text{in}} = \xi_{\text{mag}} R_{\text{mag}}, \quad \text{where} \quad R_{\text{mag}} \equiv \left(\frac{\mu^2}{\dot{M}_{\text{out}} \sqrt{GM_{\star}}} \right)^{2/7}. \quad (4)$$

One can regard parameter ξ_{mag} as the one incorporating our current uncertainty about the physics at the disc-magnetosphere boundary. There is also an issue of matching a 1D model with a real picture of asymmetric and fluctuating flows of plasma.

Estimates of ξ_{mag} obtained in 1D models are: 0.5 (Ghosh & Lamb 1979), 0.3 – 1 (Chashkina et al. 2017), $\xi_{\text{mag}} < 1.5$ and it is a function of ω_{S} (Kluźniak & Rappaport 2007). MHD simulations give $\xi_{\text{mag}} \sim 0.4 - 0.5$ (Long et al. 2005; Bessolaz et al. 2008) for fixed μ and \dot{M} , whereas a different dependence on these parameters, comparing to (4), is formulated by Kulkarni & Romanova (2013).

If the inner radius R_{in} exceeds the radius of the light cylinder

$$R_{\text{light}} = \frac{c}{\omega_{\star}}, \quad (5)$$

the quasi-stationary disc pressure cannot balance the pressure of the pulsar wind: the former decreases as R in power of $-2.5.. -3$ and the latter as R^{-2} (Shvartsman 1970; Lipunov 1992); apparently, the disc material is to be dispersed.

2.2 Accretion rate on the neutron star

The accretion rate at the disc inner boundary is determined by the disc evolution which, in turn, depends on the disc mass, viscosity, and boundary conditions. In the standard accretion regime, all the matter reaching the disc inner edge is transferred to the star (if $R_{\text{in}} < R_{\text{cor}}$).

If the disc inner radius exceeds a corotation radius

$$R_{\text{cor}} = \left(\frac{GM_{\star} P_{\star}^2}{4\pi^2} \right)^{1/3} \approx 1.7 \times 10^6 m_{1.4}^{1/3} P_{-3}^{2/3} \text{ cm}, \quad (6)$$

where $P_{-3} = P_{\star}/0.001$ s, the centrifugal force, acting on the matter rotating with $\omega_{\star} = 2\pi/P_{\star}$ in the magnetosphere, is larger than the gravitational pulling at the equator, thus inhibiting the matter falling to the neutron star.

One can imagine that a total blockage of accretion onto the neutron star occurs when R_{in} becomes equal or larger than R_{cor} . If so, the matter reaching the inner disc radius is either expelled from the system, or accumulated in the disc, or both. The former regime corresponds to a ‘propeller’ (Illarionov & Sunyaev 1975), the latter, to a so-called ‘dead disc’ (Sunyaev & Shakura 1977). However, the real geometry and physics of the problem is quite involved and it would be reasonable, and in line with various analytical and numerical results, to assume that some matter can reach the neutron star even when $R_{\text{in}} > R_{\text{cor}}$ (see Fig. 1). For example, 2D simulations of R18 show

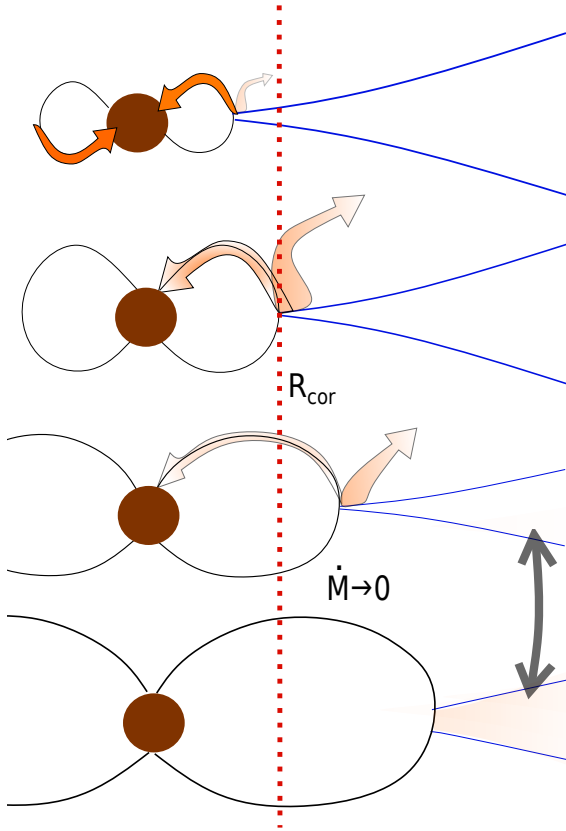


Figure 1. Illustration to the POSA scenario. The two lower pictures illustrate the propeller regime, or rather its two snapshots, assuming the oscillatory character of the accretion flow. The inner disc ‘breathes’ quasi-periodically between the two extreme states. The POSA scenario implies that some matter can outflow even when the inner disc radius $R_{\text{in}} < R_{\text{cor}}$.

that a part of the matter can flow above or below the closed part of the magnetosphere and accrete onto the star (see also [Zanni & Ferreira 2013](#)). [Güngör et al. \(2017\)](#) have suggested that a fraction of the accreted matter may be determined from an analysis of the light curves assuming that an underlying disc accretion-rate time-dependence is known. In the present study, we choose another strategy: to obtain the variation of the disc accretion rate making most simple assumptions about developments at the inner boundary.

Altogether, the matter flow can be divided in three ways: down to the neutron star, away by the propeller-mechanism, back to the disc. In our code, we introduce a penetration parameter $f_{\star} = \dot{M}_{\star}/\dot{M}_{\text{in}}$, which can be set according to different schemes³ of matter penetration (see [Table 1](#)):

- ‘SA’ There is no outflow at the magnetospheric boundary. All matter is either accreted on the star in the course of short-term events or remains in the disc. If \dot{M}_{in} is not zero then it has to fall on the neutron star.
- ‘PO’ Total screening of the neutron star by the magnetosphere if its radius exceeds the corotation radius. Then the penetration parameter is the step Heaviside function $f_{\star} = H(R_{\text{cor}} - R_{\text{in}})$.
- ‘POSA’ Gradual blocking of accretion onto the neutron star. In the present work, we use an approximation to numerical simu-

lations by [R18](#) that provides f_{\star} as a function of the fastness parameter $\omega_s \equiv \omega_{\star}/\omega(R_{\text{in}})$.

[R18](#) numerically found a time-averaged efficiency of a propeller, which depended on the poloidal wind velocity. If the accretion flow at the disc edge is split into the accretion flow onto the star and the wind, then the portion of the accretion rate onto the star is $f_{\star} = 1 - f_{\text{eff}}$, where f_{eff} is a parameter of [R18](#), which depends on the characteristic velocity of the outflowing matter regarded as the wind. If the wind contains the matter with the poloidal velocity higher than $v_{\text{min}} = v_{\text{esc}}$, where the escape velocity $v_{\text{esc}} = \sqrt{2GM_{\star}/r}$, then $f_{\text{eff}} = 0.0006 \omega_s^{4.01}$ (see [table 2 of R18](#))⁴. The portion of the propelled matter and the average velocity of the outflow become larger with increasing fastness ω_s . The fate of the lower-speed outflow is obscure; it may flow back to the disc⁵, but that was beyond the simulation region of [R18](#). Presumably, the matter outflowing from the inner boundary with a mild velocity returns back to the disc and reaches the inner boundary again after the viscous time at the radius of return. Generally, this time scale is expected to be shorter than the viscous time scale of the whole viscously-evolving disc, and such circulations are effectively averaged out in the long-time picture⁶. However, if the hot zone had small radial extent, such circulations would affect its dynamic viscous evolution.

Each of the above scenarios should be regarded as a toy model, allowing us to make conclusions about the overall disc evolution.

2.3 Torque at the inner edge of a disc

Outside the corotation radius, the magnetic torque accelerates the rotation of the matter or pushes the disc matter outward, depending on the diamagnetic properties of the disc. In either case, assuming that interaction zone is not too wide, the inner boundary condition on the viscous torque can be written as:

$$F_{\text{in}} = \kappa_{\text{td}} \frac{\mu^2}{R_{\text{in}}^3} \text{ for } R_{\text{in}} > R_{\text{cor}}, \quad (7)$$

([Davidson & Ostriker 1973](#); [Lynden-Bell & Pringle 1974](#); [Syunyaev & Shakura 1977](#); [Lipunov 1992](#); [Spruit & Taam 1993](#); [Kluźniak & Rappaport 2007](#); [Matt & Pudritz 2005](#)). Here κ_{td} is the dimensionless coefficient incorporating our uncertainty of MHD processes at the boundary between the disc and magnetosphere.

Inside the corotation radius, the magnetic torque is expected to decelerate rotation of the disc, ‘helping’ the viscosity to remove angular momentum from the matter, so that the accretion process is facilitated. Consequently, the release of the viscous heat in the disc is to be modified. The size of the region, where the disc and magnetic field effectively interact, affect the actual values of the total magnetic torque and the location of the inner disc edge (for example, [Ghosh & Lamb 1979](#); [Wang 1987, 1995](#); [Armitage & Clarke 1996](#); [Matt & Pudritz 2005](#); [Kluźniak & Rappaport 2007](#)). As an approximation for a disc with a relatively thin interaction zone, the same view of F_{in} as (7) can be adopted for the accretion regime, but with a fixed radius:

$$F_{\text{in}} = \kappa_{\text{t}} \frac{\mu^2}{R_{\text{cor}}^3} \text{ for } R_{\text{in}} < R_{\text{cor}}. \quad (8)$$

⁴ Precision of the power index is excessive in our context but we keep it identical with that in [R18](#).

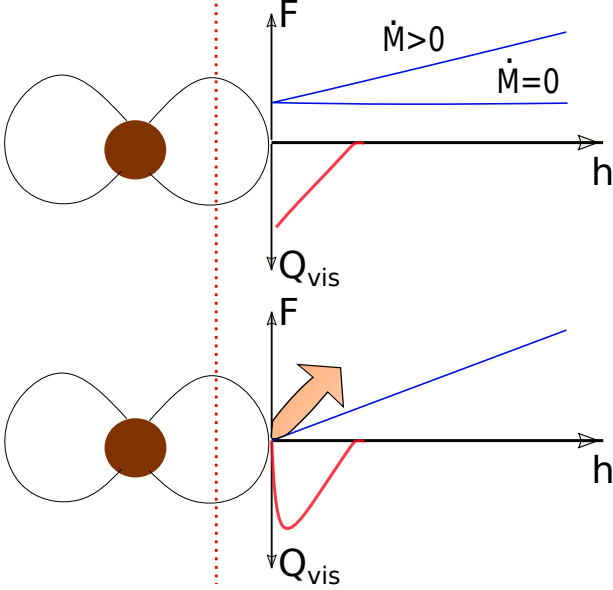
⁵ See also a discussion on failed magnetic expulsion and circulation in the disc by ([Spruit & Taam 1993](#)).

⁶ In the majority of specific models, described in §4, R_{hot} is at least two orders of magnitude larger than R_{in} when $R_{\text{in}} < R_{\text{light}}$.

³ SA – ‘star accretion’; PO – ‘propeller outflow’; POSA – both

Table 1. Reference to model scenarios of accretion onto neutron star, see §2.2 and §2.3.

Scenario	Concept	Accreted part $f_\star = \dot{M}_\star/M_{\text{in}}$	Torque coefficient	
			for $R_{\text{in}} < R_{\text{cor}}$	for $R_{\text{in}} > R_{\text{cor}}$
SA	no-outflow, everything falls onto NS	1	$\kappa_t = \xi_{\text{mag}}^{7/2}$	$\kappa_{\text{td}} = \kappa_t$
PO	propeller outflow; nothing falls onto NS if $R_{\text{in}} > R_{\text{cor}}$	$H(R_{\text{cor}} - R_{\text{in}})$	$\kappa_t = \xi_{\text{mag}}^{7/2}$	$\kappa_{\text{td}} = 0$
POSA	gradual blocking, matter partly outflows	$f_\star(\omega_s)$	$\kappa_t = \xi_{\text{mag}}^{7/2}$	$\kappa_{\text{td}} = \kappa_t$


Figure 2. Possible torque distributions $F(h)$ if $R_{\text{in}} > R_{\text{cor}}$ are shown by the blue lines. In the top plot, the case with a finite inner torque, corresponding to SA and POSA scenarios, is shown. In the lower plot, a torque distribution for the PO scenario with $\kappa_{\text{td}} = 0$ is shown. Red lines illustrate the heat radiated locally as the log-scaled distribution $\log(Q_{\text{vis}})$ vs. $\log(h)$.

This condition numerically approximates the situation of the viscous torque approaching zero, $F_{\text{in}} \rightarrow 0$, since $F_{\text{in}}/(M_{\text{in}}h_{\text{in}}) \propto \kappa_t(R_{\text{in}}/R_{\text{cor}})^3 \rightarrow 0$ for $R_{\text{in}} \ll R_{\text{cor}}$. Alternatively, as a next approximation, one could solve Eq. (1) with a radially-distributed magnetic torque to resolve the structure of the interaction zone (see the previous references).

Notice that, while the torque coefficient can be set different in (7) and (8), in the modeling below we keep $\kappa_{\text{td}} = \kappa_t$ in both SA and POSA scenarios to ensure the smoothness of a solution.

If the matter is propelled away from R_{in} , the work done by the magnetic torque can be ‘divided’ between the propelled matter and the matter remaining in the disc. Various models suggest that propelling is hardly very effective when R_{in} is not much greater than R_{cor} , and thus, generally, κ_{td} is a function of the fastness ω_s (e.g., D’Angelo & Spruit 2012, R18). For a ‘very efficient propeller’ regime (PO scenario) we set a simple condition of a zero disc torque: $\kappa_{\text{td}} = 0$.

In Fig. 2 we schematically illustrate the possible torque distributions when the inner disc radius is beyond the corotation radius. In a stationary disc without mass sinks, the radial distribution of the viscous torque is

$$F = F_{\text{in}} + \dot{M}(h - h_{\text{in}}). \quad (9)$$

The heat released in the disc can be found as $Q_{\text{vis}} = (3/8\pi)(GM_\star)^4 F/h^7$. Figure 3 shows calculated distributions of the viscous torque in a hot-zone model with varying inner and outer

radii for $\kappa_t = \kappa_{\text{td}}$. Notice that the accretion rate $\dot{M} = \partial F/\partial h$ is quasi-stationary in the inner zone (notice the log scale) and decreases with time.

In line with our simplified model, the parameter κ_t can be related to the ratio $\xi_{\text{mag}} = R_{\text{in}}/R_{\text{mag}}$ to satisfy a specific condition of a neutron star spin equilibrium. An effective formulation for the evolution of neutron star angular momentum associates the spin-up of the star with the torque added by the accreted matter, and the spin-down, with the magnetic braking (Lipunov 1981, 1982a,b, 1992):

$$\frac{dI\omega_\star}{dt} = \dot{M}_{\text{in}}\sqrt{GM_\star R_{\text{in}}} - \kappa_t \frac{\mu^2}{R_t^3}, \quad R_t = \max(R_{\text{in}}, R_{\text{cor}}), \quad (10)$$

where I is the moment of inertia of the neutron star, ω_\star is the neutron star spin velocity, \dot{M}_{in} is the accretion rate at the inner boundary of the accretion disc. Equation (10) can also be formally applied when $R_{\text{in}} \ll R_{\text{cor}}$ and there is no braking of a neutron star: since the 1st term on the r.h.s. of (10) exceeds greatly the 2nd term, the latter can remain in the sum as a non-important term.

If a neutron star is in the equilibrium, the l.h.s. of (10) is zero: the accreted angular momentum, spinning-up the star, is balanced by the negative magnetic torque, which concurrently spins down the star. According to various models, the equilibrium occurs when the inner disc radius is close but slightly less than the corotation radius (Wang 1995; Armitage & Clarke 1996; Kluźniak & Rappaport 2007; Matt & Pudritz 2005). Substituting the magnetic torque (8) as the second term in r.h.s. of (10), one obtains:

$$\frac{dI\omega_\star}{dt} = \dot{M}_{\text{in}}\sqrt{GM_\star R_{\text{in}}} \left(1 - \kappa_t \xi_{\text{mag}}^{-7/2} \left(\frac{R_{\text{in}}}{R_{\text{cor}}}\right)^3\right) \quad (11)$$

Thus for a neutron star to be in the equilibrium when $R_{\text{in}} \approx R_{\text{cor}}$, the parameters should be related as follows: $\kappa_t \approx \xi_{\text{mag}}^{7/2}$. For example, if we set $\xi_{\text{mag}} = 0.5$ then $\kappa_t \approx 0.088$.

Further, as an option, we shall study a case of a ‘left-over’ disc. For this, we shall fix some final value of the magnetospheric radius R_{dead} . The inner disc radius ‘freezes’ when it expands to the value R_{dead} and

$$F_{\text{dead}} = \kappa_{\text{td}} \frac{\mu^2}{R_{\text{dead}}^3}. \quad (12)$$

Such ‘dead’ disc, having Keplerian rotation at each radius, radiates the viscous heat, the energy for which is supplied by the neutron star rotation.

2.4 Outer radius of the hot disc and irradiation of the disc

The disc consists of two parts: the ‘hot’ ionized and the ‘cold’ neutral outer part. The irradiation of the disc affects the radius of its ionized hot part if the irradiating flux exceeds the local radiation flux due to the viscous heating:

$$Q_{\text{irr}} = C_{\text{irr}} \frac{L_x}{4\pi r^2} > Q_{\text{vis}}, \quad (13)$$

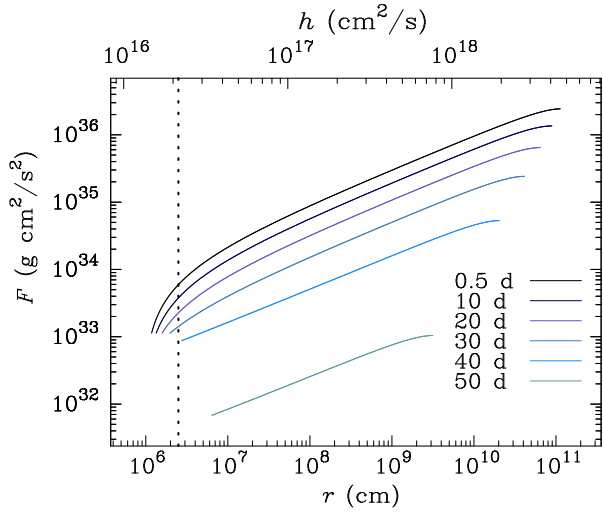


Figure 3. Torque distribution at different times marked from top to bottom. Specific angular momentum is shown at the top axis. As the luminosity and accretion rate drop, the inner radius of the disc moves away, pushed by the magnetosphere. At the same time, the outer radius of the hot zone decreases (see §2.4). Corresponding light curves are presented in Fig. 7, and the surface density, in Fig. A1. The vertical line marks the corotation radius.

where C_{irr} is a dimensionless irradiation parameter. Under the assumption that C_{irr} is constant and $L_x = \eta_{\text{accr}} \dot{M} c^2$, the ratio of these fluxes depends only on the radius:

$$\frac{Q_{\text{irr}}}{Q_{\text{vis}}} = \frac{4}{3} \eta_{\text{accr}} C_{\text{irr}} \frac{r}{R_s}, \quad (14)$$

where $R_s = 2GM_\star/c^2$ (Suleimanov et al. 2007). The ‘irradiation temperature’ can be defined as $Q_{\text{irr}} \equiv \sigma T_{\text{irr}}^4$. Following Tuchman et al. (1990); Dubus et al. (1999), we adopt the following condition to define the hot disc outer radius R_{hot} : $T_{\text{irr}} = 10^4$ K if (13) fulfills.

When condition (13) deteriorates at $R_{\text{hot}}(t)$ at some late time, the irradiation-controlled evolution is superseded by an evolution determined by the cooling-front propagation, in accordance with the DIM model (Dubus et al. 2001; Lasota 2001; Hameury 2020; see also Lipunova & Malanchev 2017). To find $R_{\text{hot}}(t)$ one can use the cooling front velocity. The cooling front velocity evolves in a complex fashion, modeled in the dedicated studies (e.g., Menou et al. 1999a). We adopt an analytic approximation to the cooling front velocities found by Ludwig et al. (1994), see their section 3. In such a framework, the front velocity depends on the values of α_{hot} and α_{cold} , mass of the central star, current radius, and the local column density. Consequently, we obtain a significant acceleration of the hot-disc boundary propagation when Q_{irr} becomes less than Q_{vis} at R_{hot} .

Thus, irradiation parameter has a great effect on the disc long-term dynamical evolution. The following analytic expression (e.g., Suleimanov et al. 2007)

$$C_{\text{irr}} = (1 - A) \Psi(\theta) \frac{z_0}{R} q, \quad \text{where } q = \left(\frac{d \ln z_0}{d \ln r} - 1 \right) \quad (15)$$

could be used to estimate C_{irr} in (13), where $(1 - A)$ is the portion of absorbed and thermally reprocessed incident flux, z_0 is the semithickness of the disc, and $\Psi(\theta)$ is the angular distribution of the irradiating flux, where θ is the angle between a ray from the centre and the normal to the disc. For the gas-pressure dominated, absorption-opacity zone (with the Kramers law) of the disc, $q = 1/8$ (e.g., Shakura & Sunyaev 1973).

Unfortunately, a problem with estimate (15) is that resulting C_{irr} is too low, if one considers direct irradiation of the photosphere of a standard disc. For example, (Suleimanov et al. 1999) estimated $(1 - A) \sim 0.1$. Substituting $z_0/r = 0.06$ into (15), we get $C_{\text{irr}} \approx 7.5 \times 10^{-4}$. On the other hand, it is well established (e.g., Suleimanov et al. 2008) that C_{irr} must be larger to explain optical flux of LMXBs. A hypothesis was proposed that an extra scattering occurs in the medium above the disc and enhances the irradiation factor. Mescheryakov et al. (2011) considered the radiation transfer problem for a disc with an extended atmospheric layer around a neutron star. They assumed that the disc was irradiated by the central flux from the neutron star with $L = \eta_\star \dot{M} c^2$ with the accretion efficiency $\eta_\star = 0.1$ and angular distribution $\Psi(\theta) = 1$. Following the graphical results of their figure 8 and taking into account (14), we deduce that the characteristic value of $C_{\text{irr}} \approx (4 - 8) \times 10^{-3}$ for $L \approx L_{\text{Edd}}$ and $C_{\text{irr}} \approx (2.6 - 3.5) \times 10^{-3}$ for $L \approx 0.1 L_{\text{Edd}}$ at $R \sim 10^{11}$ cm.

One can use the optical data to constrain C_{irr} . This is what we do for Aql X-1 in the course of data fitting. We take into account the fact that the angular distribution of the X-ray flux from the star differs from that of the flux coming from the central disc. We assume that the star radiates isotropically, $\Psi(\theta) = 1$. For radiation from the disc, we take $\Psi(\theta) = 2 \cos(\theta) \approx 2 z_0/r$ (e.g., Suleimanov et al. 2007), assuming that the central part of the disc lie in the equatorial plane of the outer disc.

In the model we set two different parameters \tilde{C}_{irr} , for the cold and hot part of the disc, which relate to parameter C_{irr} from (13) as follows

$$C_{\text{irr}} = \tilde{C}_{\text{irr}} \left(\frac{z_0/r}{0.05} \right)^k \Psi(\theta), \quad k = 1; \quad (16)$$

$$C_{\text{irr}}^{\text{cold}} = \tilde{C}_{\text{irr}}^{\text{cold}} \Psi(\theta).$$

Both disc parts can contribute to the optical flux. However, only the ‘hot’ part of the disc (with $T_{\text{eff}} > 10^4$ K) is involved in the fast viscous evolution; moreover, its size determines the global viscous time, i.e., the rate of the evolution. The viscous evolution in the colder part proceeds on a much longer viscous time scale because the temperature and viscosity are lower there. Additionally, slower evolution may be explained by suggested lower values of α in the disc with recombined material (e.g., Smak 1984). At the outer boundary of the hot part we assume $\dot{M} = 0$ (Lipunova & Malanchev 2017). Comparing to models with a resolved cooling front structure (e.g., Dubus et al. 2001), our simple approach may result in a skewed estimate of the parameter α .

2.5 Observed flux from the disc and neutron star

Thermalization of the incident flux in the disc upper layer leads to the enhancement of the local black-body radiation. Subsequently, the local effective temperature can be expressed as

$$T_{\text{eff}}^4 = T_{\text{irr}}^4 + T_{\text{vis}}^4. \quad (17)$$

Observed spectral flux is calculated taking into account possible color correction:

$$\mathcal{F}_{\nu, \text{disc}} = \int I_\nu d\Omega = \frac{2\pi \cos i}{d^2 f_{\text{col}}^4} \int_{R_{\text{in}}}^{R_{\text{out}}} r B_\nu(f_{\text{col}} T_{\text{eff}}(r)) dr, \quad (18)$$

where $d\Omega = 2\pi r dr \cos i/d^2$ is the solid angle, at which an observer sees a disc ring, i is the disc inclination to the line of sight, d is the distance to the source, T_{eff} is obtained according to (17), and I_ν is the ring intensity. In the photosphere of the disc electron scattering can modify the blackbody spectrum (Shakura & Sunyaev 1973; Taam &

Meszaros 1987). The color correction factor f_{col} approximate effects of electron scattering in the disc photosphere Shimura & Takahara (1995); Davis et al. (2005): $I_{\nu} = B_{\nu}(f_{\text{col}} T_{\text{eff}})/f_{\text{col}}^4$. Color correction factor f_{col} is set to unity for the optical and IR bands and to 1.7, for X-ray. We ignore effects of irradiation when calculating flux in an X-ray band.

The viscous heat flux determines T_{vis} as follows:

$$\sigma T_{\text{vis}}^4 = \frac{3(GM_{\star})^4 F}{8\pi h^7}, \quad (19)$$

where the torque F is taken as the solution to the viscous evolution equation (1). In the central parts of the disc, the heat released by the viscosity dominates largely any irradiation.

For the hot part of the disc, we calculate (18) between R_{in} and R_{hot} , and for the cold part, between R_{hot} and the tidal radius R_{tid} , where R_{tid} equals 90% of the Roche lobe radius, close to the result by Papaloizou & Pringle (1977). For the cold part of the disc we take $T_{\text{vis}} = 0$ in (17) since we are not interested in the solution for the vertical structure of the cold disc. Its relative semithickness is a parameter of FREDDI and is set to 0.05 in the current work. All connected uncertainty is believed to be parametrized by $\tilde{C}_{\text{irr}}^{\text{cold}}$.

The bolometric luminosity of a viscously-heated disc can be found by integrating the radiative flux (19) over the disc surface. Since the main energy release takes place close to the centre, we can substitute the outer radius by infinity. Notice also that close to the centre the stationary solution (9) holds very accurately. One arrives at: (9):

$$L_{\text{disc}} = \left(F_{\text{in}} + \frac{\dot{M}_{\text{in}} h_{\text{in}}}{2} \right) \times \omega_{\text{in}} \quad (20)$$

in the Newtonian case, where ω_{in} is the Keplerian frequency at the inner edge of the disc, and $h_{\text{in}} = \omega_{\text{in}} R_{\text{in}}^2$. Subsequently, disc accretion efficiency is

$$\eta_{\text{disc}} = \frac{F_{\text{in}} \omega_{\text{in}}}{\dot{M}_{\text{in}} c^2} + \frac{GM_{\star}}{2R_{\text{in}} c^2}. \quad (21)$$

In the Newtonian mechanics, the accretion efficiency of the neutron star $\eta_{\star} \equiv L_{\star}/\dot{M}_{\star}/c^2$ is found assuming that the kinetic energy of radial motion of matter at the star surface is converted to radiation:

$$\eta_{\star} = \frac{R_s}{2R_{\star}} \left(1 - \frac{R_{\star}}{R_{\text{in}}} \right) + \frac{R_s}{4R_{\text{in}}} \left[1 - 2\omega_s + \omega_s^2 \left(\frac{R_{\star}}{R_{\text{in}}} \right)^2 \right], \quad (22)$$

where $\omega_s \equiv \omega_{\star}/\omega_{\text{K}}(R_{\text{in}})$ (see Appendix B).

We assume that the emitting region occupies some part of the neutron star surface, $S_X/(4\pi R_{\star}^2)$, and the spectrum is black-body. The effective temperature of this region is $T_{\star} = [L_{\star}/(\sigma_{\text{SB}} S_X)]^{1/4}$. If the radiation is isotropical, the observed flux density is

$$\mathcal{F}_{\nu, \star} = \frac{S_X}{4\pi d^2} \pi B_{\nu}(T_{\star}). \quad (23)$$

Since we are interested in burst light curves, that is, in the flux variations over time of days, the possible oscillations on time scales $\ll 10^4 - 10^5$ s are smoothed out. In other words, the accretion rate in (20) and (B1) is an ‘average’ value determined by the viscous evolution of the disc, i.e., by the solution to equation (1).

2.6 Flux from the companion star

Our code calculates orbit-modulated light curves of the companion star, irradiated by X-rays. Fig. 4 presents a visualization of the resulted effective temperature on the disc and the optical star in Aql X-1. The effective temperature of the disc is calculated according to (17), and

$$T_{\text{eff}}^4 = T_{\text{irr}}^4 + T_{\text{opt}}^4. \quad (24)$$

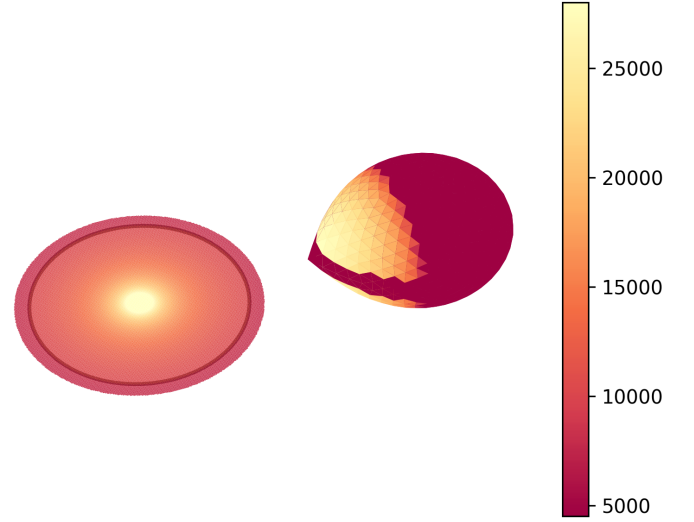


Figure 4. Visualization of the binary system with the parameters listed in Table 2 and accretion rate equal to the peak one in model SA1 (see Table 3). The circle on the disc shows the border between hot and cold zones. Effective temperature is color-coded.

for the star, where T_{opt} is the effective temperature of a non-irradiated star, and

$$\sigma T_{\text{irr}}^4 = \frac{(1 - a_{\text{opt}})(L_{\text{disc}} \Psi(\theta) + L_{\star})}{4\pi r^2} \cos \xi, \quad (25)$$

where a_{opt} is the star’s bolometric albedo, r is the distance between the neutron star and a point on the surface of the optical star, and ξ is the angle between the direction to the neutron star and normal to the optical star surface. Other designations are as in §2.4. The star surface is calculated using the Roche lobe filling factor $R_{\text{pol}}/R_{\text{pol}}^{\text{Roche}}$ (Antokhina 1988). Resulting orbit-modulated light curves were compared with those obtained by a more sophisticated code, developed for a twisted disc in Kolesnikov et al. (2020), and demonstrated an agreement to an accuracy of 5%.

3 MULTIWAVELENGTH DATA OF THE AQL X-1 OUTBURST IN 2013

Table 2 summarizes parameters which we use for modeling of the 2013 outburst in Aql X-1. When references are given, we adopt the values from previous modelings or the values lying in the observational limits. For example, Mata Sánchez et al. (2017) using their near-infrared observations refined T_0 and the orbital period P_{orb} and gives estimates of distance $d = 6 \pm 2$ kpc, mass ratio 0.41 ± 0.08 , inclination $36^\circ < i < 47^\circ$ and spectral class of the donor $K4 \pm 2$. We assume $d = 5$ kpc following Meshcheryakov et al. (2018).

Figures 5 and 6 show the observed evolution during the outburst of Aql X-1 in 2013 observed by Swift/XRT, Swift/UVOT, and SMARTS/IR. A description of Swift/XRT light curves production can be found in Evans et al. (2007). We performed spectral fits to Swift/XRT data in 0.5–10 keV using a model of a black-body plus a power-law tail (see §3.1 and Fig. A2). In the optical, we made magnitude–flux transformation, using passbands zero points given in Table 4 of Meshcheryakov et al. (2018) (see §3.2).

Table 2. Fixed parameters of the model of Aql X-1.

Variable	Parameter	Value	Ref.
M_{\star}	NS mass	$1.4 M_{\odot}$	
R_{\star}	NS radius	1.12×10^6 cm	
ν_{\star}	NS spin frequency	550 Hz	(1)
R_{cor}	Corotation radius	2.5×10^6 cm	Eq. (6)
R_{light}	Light cylinder radius	8.7×10^6 cm	Eq. (5)
R_{tid}	Tidal radius of the disc	$0.9R_{L1} = 1.87R_{\odot}$	(2)
P_{orb}	Orbital period	0.7895126	(1)
T_0	Ephemeris	2455810.387 d	(3)
q	Mass ratio	0.39	(3,4)
a	Semi-axis	$4.5 R_{\odot}$	
M_{opt}	Optical star mass	$0.55 M_{\odot}$	
T_{opt}	Optical star temperature	4500 K	(3)
a_{opt}	Optical star albedo	0.5	(5)
$R_{\text{pol}}/R_{\text{pol}}^{\text{Roche}}$	Roche lobe filling	1	
d	Distance to the source	5 kpc	(3,4,6)
i	Inclination of the orbit	40°	(3)
$E(B - V)$	Color excess	0.64 ± 0.04	App.C
ξ_{mag}	$R_{\text{in}}/R_{\text{mag}}$	0.5	Eq. (4)
κ_t	Magnetic torque coef.	$\xi_{\text{mag}}^{7/2} \approx 0.088$	§2.3
f_{col}	Inner disc color correction	1.7	§2.5
$S_X/(4\pi R_{\star}^2)$	Hot spot fraction	0.4	§2.5
$(z/r)_{\text{cold}}$	Outer disc relative semithickness	0.05	

(1) White & Zhang (1997); Zhang et al. (1998b); Casella et al. (2008); (2) Papaloizou & Pringle (1977); (3) Mata Sánchez et al. (2017); (4) Meshcheryakov et al. (2018); (5) Basko et al. (1974); (6) Galloway et al. (2008)

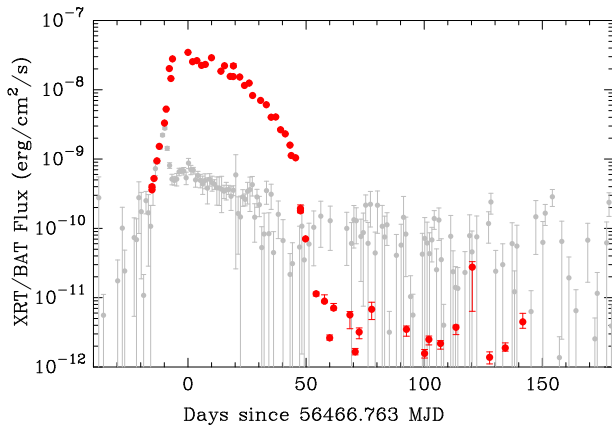


Figure 5. Red circles show unabsorbed total flux in 0.5 – 10 keV, observed by Swift/XRT in ‘wt’ and ‘pc’ mode. The flux is calculated using spectral fitting by model $\text{tbabs}*(\text{bbody}+\text{powerlaw})$ in XSPEC12.10.0c (see §3.1). Grey data points show absorbed 15–50 keV Swift/BAT counts converted to absolute units using Crab (see §3.1).

3.1 Swift X-ray data

Spectra, produced by the automatic pipeline in 0.3 – 10 keV (Evans et al. 2009), as well background, and ancillary response files were obtained from the UK Swift Science Data Centre using the Swift-XRT data products generator⁷. These spectra were rebinned so they had minimum of 1 count in each bin. Subsequently, we have performed spectral modelling by black-body and power-law components in XSPEC12.10.0c for observations in ‘wt’ and ‘pc’

⁷ www.swift.ac.uk/user_objects

mode for 0.5–10 keV using the C-statics. For the absorption we set $\text{abund} = \text{wilm}$, and photoionization cross-sections $\text{xsect} = \text{vern}$. The unabsorbed flux in 0.5–10 keV is calculated using model $\text{tbabs}*\text{cflux}(\text{bbody}+\text{powerlaw})$. Uncertainty ranges ($1-\sigma$) on the intrinsic flux are obtained by the Markov-Chain Monte-Carlo simulations.

Red circles in Fig. 5 show resulting evolution of the total intrinsic flux when all spectral parameters are free to vary. Fig. A2 shows the evolution of the best-fit spectral parameters. It demonstrates that before the 50th day the values of n_{H} and the photon index were relatively stable.

To assess a contribution from harder X-ray radiation, we follow the procedure of Meshcheryakov et al. (2018). We have downloaded daily light curves of Aql X-1 from Swift/BAT Hard X-ray Transient Monitor archive website⁸. For counts-to-flux conversion, we assume that 1 Crab equals to $0.220 \text{ counts s}^{-1} \text{ cm}^{-2}$ in the 15 – 50 keV band. Fig. 5 clearly indicates that before the ~ 50 th day after the peak the X-ray flux is dominated by the soft component.

3.2 Optical, UV, and IR data

The Swift/UVOT observations during the whole period of Aql X-1 accretion outburst of 2013, in *V*, *B*, *U*, *UVW1*, *UVW2*, and *UVM2* are shown in Fig. 6. Errors are purely statistical and correspond to $1-\sigma$ confidence level. For the data reduction, images initially pre-processed at the Swift Data Center at the Goddard Space Flight Center were used. Subsequent analysis was done following procedure described at the web-page of UK Swift Science Data Centre⁹. Namely, photometry was performed using `uvotsource` procedure with the source apertures of radius 5 and 10 arcsec for the background for all filters. The 5 arcsec aperture contains flux from the group of faint stars, located nearby to the Aql X-1 optical counterpart.

The 1.3-m telescope at Cerro Tololo (Chile) monitored Aql X-1 in *R* and *J* bands on a regular basis. We use a publicly available¹⁰ SMARTS light curves in our analysis. The photometric reduction procedure was performed by the Yale SMARTS XRB team, following the reduction steps described in Buxton et al. (2012).

Using zero points of the passbands, which can be found in Meshcheryakov et al. (2018), and the optical extinction to Aql X-1 $E_{B-V} = 0.64 \pm 0.04$ (see Appendix C), the magnitudes were converted to the flux density units. They are compared to modeled \mathcal{F}_{ν} , calculated at $\nu = c/\lambda_{\text{eff}}$, where λ_{eff} are the effective wavelengths (Meshcheryakov et al. 2018).

4 RESULTS

We have performed numerous fits to the observed light curves of the 2013 burst decay of Aql X-1 by the model light curves produced with the modified FREDDI-code. For fitting, the data in 0.5 – 10 keV and *U*, *B*, *V*, and *R* in the interval between MJD 56465.763 and MJD 56516.533 (between the peak and 53th day after the peak) is used. Resulting models are plotted for a longer time interval, see, for example, Fig. 7 and figures in the Supplement Material, and also for *J* and *UVM2* data. Table 3 summarizes essential results. For models SA11 and SA12, we fit data before the 135th day. In this case all X-ray points after the 53th day are substituted by one point,

⁸ swift.gsfc.nasa.gov/results/transients/index.html

⁹ www.swift.ac.uk/analysis/uvot/index.php

¹⁰ www.astro.yale.edu/smarts/xrb/home.php

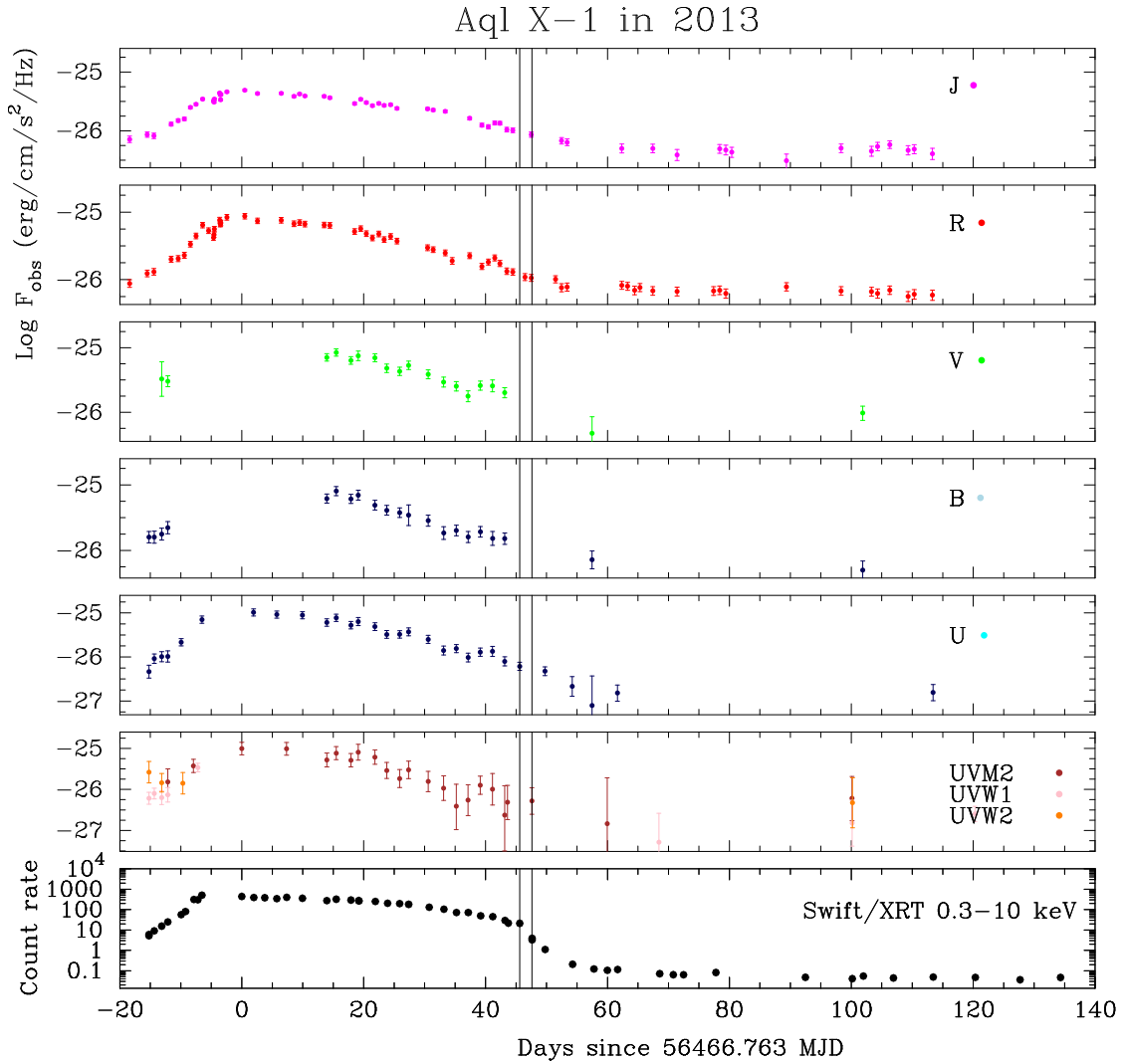


Figure 6. From top to bottom: logarithm of dereddened flux density, SMARTS/IR (J and R) and Swift/UVOT (V , B , U , and ultraviolet bands), the Swift/XRT 0.3–10 keV light curve as counts/sec, ‘wt’ and ‘pc’ mode. The zero time is set to MJD 56466.763 (23 Jun 2013). Two vertical lines mark the ‘knee position’ – the time interval when the X-ray flux starts to drop rapidly.

obtained from the spectrum integrated in the interval MJD 56550–56650 – the point with a long horizontal bar in Fig. A2. In the rest of the models, down starting from PO13, we fit the data in interval MJD 56465.763–56530.763 (before the 65th day).

Our fitting procedure provides estimates of the following parameters: the peak accretion rate, α -parameter in the hot disc, irradiation parameter C_{irr} , magnetic field of the neutron star, whereas we fix value of ξ_{mag} and a_{opt} . These parameters are interrelated. In particular:

- α and C_{irr} affect the overall rate of the source evolution;
- B_x and ξ_{mag} affect the knee position;
- C_{irr} , $C_{\text{irr}}^{\text{cold}}$, and a_{opt} affect the optical to X-ray flux ratio.

A performance of a particular model can be assessed by its χ^2 or \mathcal{R}^2 (the coefficient of determination¹¹). For the optical data (U , B , V ,

¹¹ $\mathcal{R}^2 = 1 - \frac{\sum (y_i - m(t))^2}{\sum (y_i - \bar{y})^2}$ measures how well observed data are replicated by the model, where y_i is the data, $m(t)$ is the model, \bar{y} is the mean of y_i . The model prognosis is perfect when $\mathcal{R}^2 = 1$.

and R), values of χ^2 are calculated for the orbit-averaged total flux. The statistics are calculated for interval 0–53 d for all fits; there are 27 X-ray and 81 optical points in the interval.

The nature of the data is so that a lot of local minima of the fit statistic exist. Thus it is impossible to circle out a single best model. Still, let us consider a particular model in order to compare others to it.

4.1 A particular model

In Figure 7 model SA1 is presented when the shrinking of the hot zone drives the X-ray flux drop around the 35th day. The inner radius of the disc levels with the corotation radius at 37.45 day at $\dot{M}_{\text{in}} \approx 5.3 \times 10^{16}$ g/s when $R_{\text{hot}} \approx 2 \times 10^{10}$ cm and the bolometric luminosity of the star and disc is 9.2×10^{36} erg/s for the total accretion efficiency $\eta \approx 0.19$. In the 1st and 2nd panel of Fig. 7, the shaded rectangles show the stages when the inner disc radius is larger than the corotation radius R_{cor} (rectangle marked with letter ‘c’); when the inner disc radius is larger than the light-cylinder radius R_{light} (letter ‘l’); when the irradiation-to-viscous flux ratio $Q_{\text{irr}}/Q_{\text{irr}} < 1$ at R_{hot} and the radius

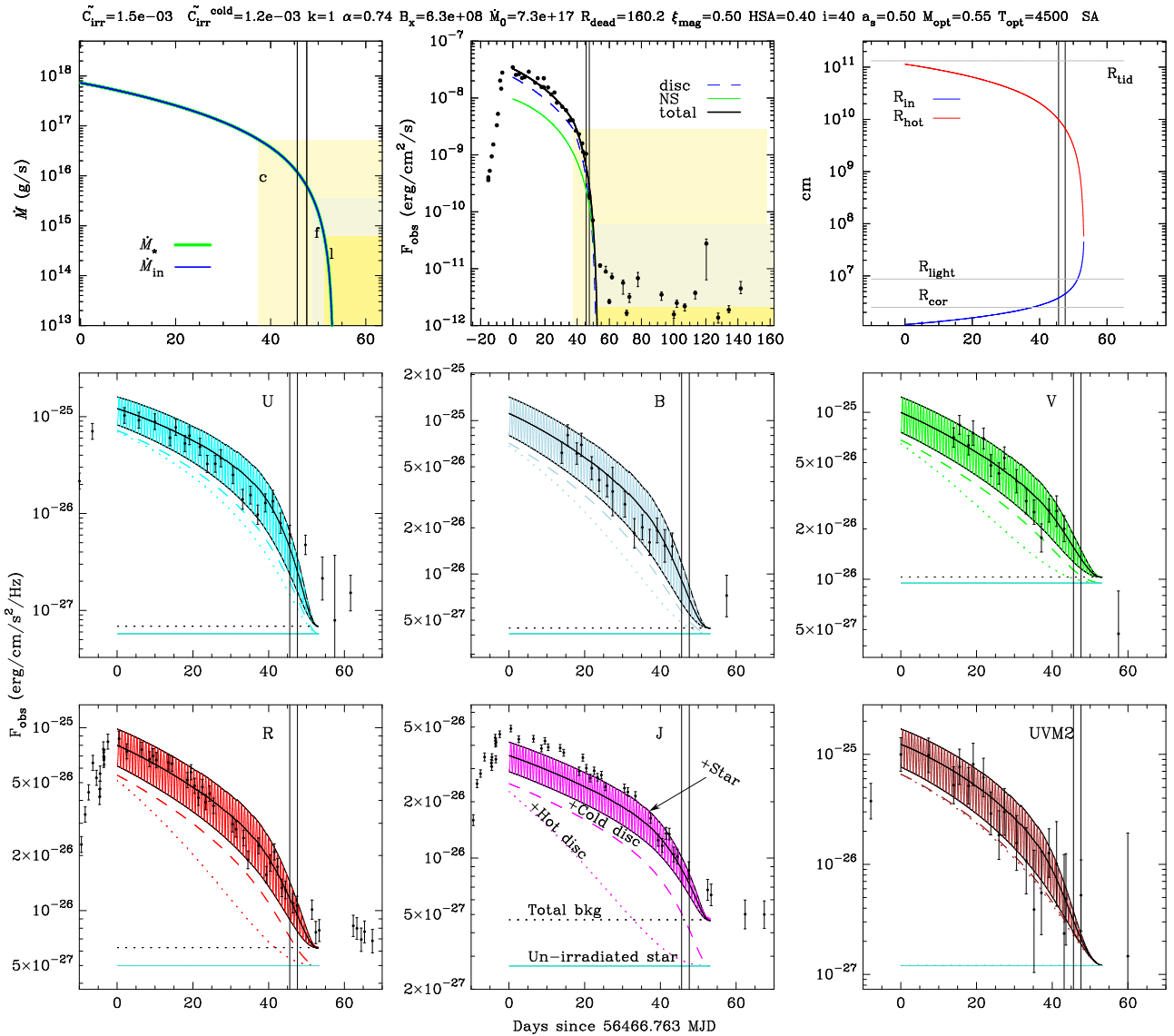


Figure 7. Model SA1 and observed light curves. The fit parameters are shown at the top and in Table 3. From left to right, from top to bottom, the panels are: accretion rate, unabsorbed X-ray flux, disc radii, dereddened flux density at λ_{eff} of *U*, *B*, *V*, *R*, *J*, and *UVM2*. In the 1st and 2nd panel, the colored areas mark stages of evolution (see description in the text, §4.1). In the 3rd panel, the horizontal lines show the corotation radius, light-cylinder radius, and tidal radius. In the panels with the optical flux, a dotted curve is the hot disc emission, a dashed curve is the hot+cold disc emission. The oscillating curves additionally include the orbit-modulated light from the optical companion. The horizontal dotted line is the background level, which is the sum of the flux from the secondary star during quiescence (calculated in the model; the solid horizontal line) and the sky background.

of the hot disc R_{hot} is found using the front velocity, as described in §2.4 (letter ‘f’).

In this particular model, no outflow is present, and the accretion onto the neutron star should continue after 37.45 day in a sporadic fashion. The low-level X-ray plateau after the 55th day is not addressed in this model¹².

It is interesting that, contrary to a primary expectation, the X-ray flux detected by an observer is dominated by the disc, which is roughly twice as brighter comparing with the flux from the neutron star. This is explained by (i) a rather fast rotation of the star yielding

the bolometric luminosity of the disc about 60% brighter than that of the star; (ii) the angular distribution of the disc emission $\Psi(\theta) = 2 \cos \theta$ causes the mild enhancement at $\theta = i = 40^\circ$, comparing to an isotropic case.

Figure 8 shows corresponding evolution of some key dimensionless parameters: accretion efficiency (in the disc and on the star); the disc semithickness z_0/r , irradiation-viscous-flux ratio $Q_{\text{irr}}/Q_{\text{vis}}$ at the outer radius of the hot zone, the fastness parameter $\omega_s = \omega_\star/\omega_K(R_{\text{in}})$, the accretion penetration parameter $f_\star = \dot{M}_\star/\dot{M}_{\text{in}}$; the irradiation parameters applicable to the hot/cold disc for the flux from disc/star. Note that irradiation parameter for the cold disc does not vary since its semithickness is fixed.

¹² Note that whenever the inner disc radius becomes greater than the radius of the light cylinder, the material of the disc is dispersed by the pulsar wind, at least, in its hot part, and the model solution is purely formal for those times.

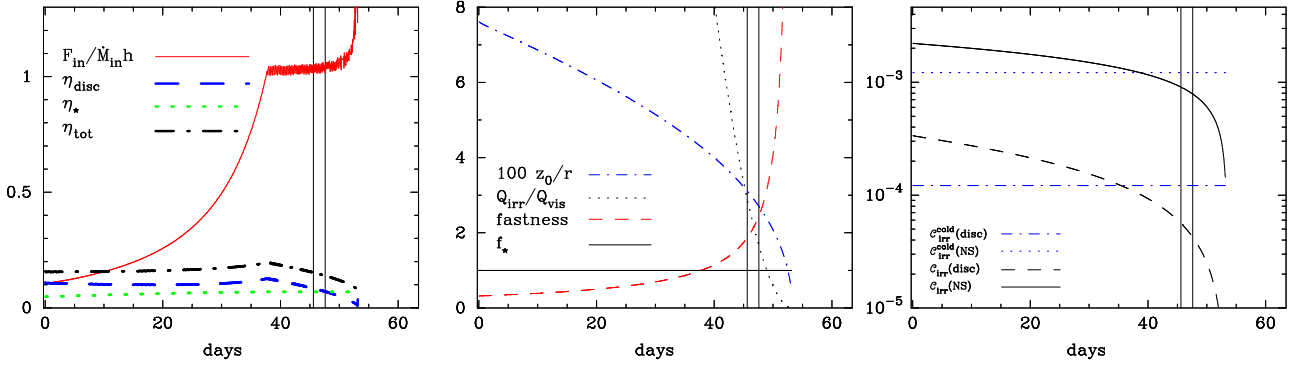


Figure 8. Evolution of key dimensionless values for model SA1, see Fig. 7. In the left panel: solid line is the modulus of the ratio of the spin-down to spin-up torque acting on the neutron star (as prescribed by Eq. (10)); other curves show accretion efficiency in the disc and at the neutron star, and their sum. In the middle panel: relative semithickness of the hot disc at R_{hot} , multiplied by 100, irradiation-to-viscous-heat ratio at R_{hot} , fastness parameter ω_s , and ratio f_* of the accretion rate onto the star’s surface to the accretion rate in the disc at R_{in} . The right panel: irradiation parameters C_{irr} and $C_{\text{irr}}^{\text{cold}}$ defined by (16); in the brackets the source of X-ray radiation is indicated.

Table 3. Parameters of resulting models. Columns are: (1) Figure number; (2-6) Resulting parameters; (7) Parameter restrictions or changes to values given in Table 2; (8-10) Resulting χ^2 and \mathcal{R}^2 for X-ray and optical data; (11) Model ID. For the ‘POSA’ scenario, the material with $v < v_{\text{esc}}$ falls onto NS and there is no outflow when the disc reaches the star surface.

Fig	B_x (Gs)	\dot{M}_0 (g/s)	α	\tilde{C}_{irr}	$\tilde{C}_{\text{irr}}^{\text{cold}}$	Comment	χ^2 (X)	\mathcal{R}^2 (X)	χ^2 (opt)	Model ID
No outflows										
7	6.3e+08	7.3e+17	0.74	1.5e-03	1.2e-03	$\alpha \geq 0.5$	21348	0.986	155	SA1
SF??	5.2e+08	7.9e+17	0.11	1.3e-04	1.6e-03	$\alpha \leq 0.5$	21395	0.988	186	SA2
SF??	6.2e+08	9.6e+17	0.10	1.2e-04	1.7e-03	$k = 0$	52435	0.971	127	SA3
SF??	5.3e+08	8.4e+17	0.69	1.3e-03	0.0e+00	fixed $\tilde{C}_{\text{irr}}^{\text{cold}} = 0$	20805	0.986	306	SA4
SF??	7.0e+08	9.6e+17	1.59	3.8e-03	0.0e+00	fixed $\tilde{C}_{\text{irr}}^{\text{cold}} = 0, a_{\text{opt}} = 1$	35387	0.982	571	SA5
SF??	5.3e+08	7.9e+17	0.11	1.3e-04	3.8e-03	$a_{\text{opt}} = 1$	21406	0.988	193	SA6
SF??	1.0e+02	1.1e+18	0.68	1.3e-03	5.5e-04	fixed $B_x, \alpha \geq 0.5$	34573	0.979	162	SA7
SF??	1.0e+02	9.8e+17	0.13	1.6e-04	1.2e-03	fixed $B_x, \alpha \leq 0.5$	32725	0.981	177	SA8
SF??	5.5e+08	8.1e+17	0.56	9.7e-04	1.4e-03	Partial outflow if $R_{\text{in}} > R_{\text{cor}}$	20469	0.986	175	POSA9
10	3.6e+08	7.1e+17	0.53	1.2e-03	1.0e-03	Complete outflow if $R_{\text{in}} > R_{\text{cor}}$	49943	0.967	249	PO10
Dead disc for a plato, which is one point in X:										
11	3.3e+07	9.0e+17	0.29	5.2e-04	1.1e-03	B_x explains plato, $R_{\text{dead}} = R_{\text{cor}}$	21647	0.948	163	SA11
11	6.3e+08	7.3e+17	0.74	1.5e-03	1.2e-03	$R_{\text{dead}} \approx 3.3R_{\text{cor}}$ explains plato in SA1	21348	0.986	155	SA12
No disc irradiation:										
12	3.3e+08	8.2e+17	0.06	1.0e-10	0.0e+00	fixed $\tilde{C}_{\text{irr}} = \tilde{C}_{\text{irr}}^{\text{cold}} = 0$ and B_x ;	55158	0.981	1574	PO13
12	6.0e+02	1.5e+18	0.06	1.0e-10	0.0e+00	fixed $\tilde{C}_{\text{irr}} = \tilde{C}_{\text{irr}}^{\text{cold}} = 0$;	334770	0.874	1250	PO14
No irradiation and constant outer radius $R_{\text{hot}} = R_{\text{tid}}$										
12	4.2e+08	1.3e+18	4.00	1.0e-10	0.0e+00	fixed $\tilde{C}_{\text{irr}}, \tilde{C}_{\text{irr}}^{\text{cold}}$ & R_{hot}	423694	0.830	2137	PO15
12	1.0e+06	2.2e+18	4.00	1.0e-10	0.0e+00	fixed $\tilde{C}_{\text{irr}}, \tilde{C}_{\text{irr}}^{\text{cold}}, B_x$ & R_{hot}	907624	0.622	1990	PO16
Irradiation of hot disc with constant outer radius $R_{\text{hot}} = 10^{10}$ cm, no cold disc										
SF??	3.3e+08	3.6e+18	0.07	1.0e-10	2.4e-03	fixed $\tilde{C}_{\text{irr}}^{\text{cold}} = 0$ and B_x	969733	0.717	3212	PO17
Irradiation of whole disc; hot part has constant outer radius										
SF??	3.3e+08	3.4e+18	0.07	5.0e-02	1.3e-05	fixed $B_x, R_{\text{hot}} = 10^{10}$ cm	966438	0.717	2121	PO18
SF??	3.3e+08	3.3e+17	4.00	1.7e-03	1.2e-05	fixed $B_x, R_{\text{hot}} = R_{\text{tid}}$	1528271	0.512	1823	PO19

4.2 Turbulence parameter and irradiation parameter

To begin with, we set a high/low limit for a free parameter α at 0.5 (keeping other settings the same). It turns out that the resulting models behave similarly and yield comparable fit statistic (see models SA1 and SA2, Fig. 10, left panels). It can be seen (Table 3) that the rate of evolution in discs with different α is the same because the irradiation parameter is properly adjusted.

Fitting X-ray data alone, a relation between α and C_{irr} can be found. This relation between the maximum irradiation parameter C_{irr} (i.e., at the peak of the burst, see (16)) and α for models from Table 3 is shown

in Fig. 9. The degeneracy between them can be partly resolved by determining C_{irr} from the optical data. Ignoring optical contribution from other sites (the cold disc and optical companion) results in a larger hot disc. Herewith, the X-ray light curve fit becomes worse by almost two times and estimated $\alpha > 1$ (model SA5).

It should be noted here that the α -parameter, found by fits, is model-dependent. First, a method to estimate α from the dynamical evolution of the disc, ignoring winds from the disc surface that speed up the evolution, overestimates α . Second, α depends on the hot-zone

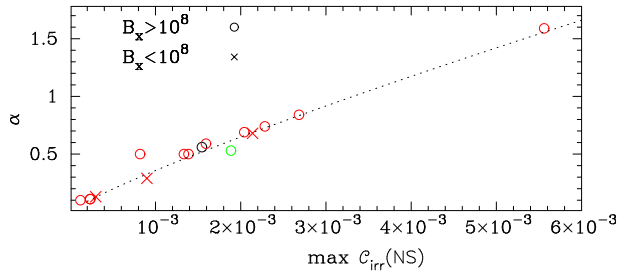


Figure 9. Relation between α and maximum irradiation factor that parametrizes the reprocessed X-ray flux emitted by the neutron star for the models listed in Table 3. Red color marks the SA scenario, black POSA, and green PO.

radius definition, which is rather simple in the present version of our scheme, see §2.4.

For the models with $\alpha > 0.5$, the value of α_{cold} (we take 0.01) does not affect the fits, since the irradiation controls practically the whole time interval used for fitting. This value affects the velocity of the cooling front and affects fitting results if \dot{C}_{irr} and α are relatively small.

We also test the properties of irradiation. Model SA3 (Fig. 10, the left panels) has the irradiation parameter that does not depend on the disc thickness ($k = 0$ in (16)) and its X-ray fit is about 2.5 times worse than that for SA1. Thus the variable irradiation parameter is favoured by our analysis (see the right panel of Fig. 8). This variability is a geometrical effect, since it ensues from changing disc thickness.

4.3 Optical flux

In our model, not only the hot ionized disc, but also the outer cold ring and the optical companion can contribute to the optical flux of the source. The total optical flux is calculated as the sum of the source flux and a ‘sky background’. The sky background is calculated as the quiescent optical flux (Meshcheryakov et al. 2018; table 4) minus the flux of the non-irradiated optical star. The flux of the non-irradiated companion depends on the chosen parameters of the binary (temperature T_{opt} , binary semi-axis a , mass ratio q , filling factor $R_{\text{pol}}/R_{\text{pol}}^{\text{Roche}}$, and inclination i , see Table 2). For chosen parameters, radius of the optical star’ is about $0.3 a$. Due to the orbital variation of the visible area of the irradiated surface of the star, the resulting optical light curves look very dense (as in two lower rows in Fig. 7).

At the end, such modeling of optical data turns out to be partly successful. On one hand, the level and trend of the optical flux are explained better with the inclusion of the cold disc and the optical star than without. This inference can be made on inspecting the optical χ^2 -values in Table 3 and the optical light curves in the Supplement Material (compare models SA4, SA5, and SA6 with model SA1). On the other hand, we could not explain fully the oscillations of the optical data by the orbit-modulated flux from the optical star. This is maybe partly due to the fact that, in addition to period-modulated fluctuations, there are fluctuations in the illuminating X-ray flux (similar to those seen in the X-ray curve), not accounted for in our modeling. Also, the amplitude of the model optical fluctuations is generally larger than observed. This may indicate that the albedo value 0.5 is an underestimation, or that the shadow on the star is actually bigger than what the model disc produces.

4.4 Magnetosphere-disc interaction

Concerning the resulting light curves, two scenarios, the one without outflows (SA) and the one that adopts results of MHD simulations by R18 (POSA), provide very similar results (compare models SA1 and POSA9). The latter describes a gradual propeller turn-on, and the similarity is due to the fact that the adopted dependence for a propelled mass portion $f_{\text{eff}}(\omega_s)$ holds for outflows with velocity greater than the escape velocity, ensuring the loss of mass from the disc. The dependence on the fastness has a high power index (about 4, see §2.2 and R18) and f_{eff} differs very little from 1 just after the inner disc edge recedes beyond the corotation radius, before the 50th day, see Fig. SF???. Overall, until the moment when the disc edge levels with the light cylinder radius, only about 10^{20} g is propelled away in model POSA9.

Comparing different scenarios of accretion inhibition near the corotation radius (Fig. 10, the right panels), we see that a model with a very efficient propeller (PO10) fits worse X-ray data because it produces a too dramatic drop, which is not observed. Thus, a scenario with a gradual decrease of the averaged accretion rate on the neutron star surface, like SA or POSA, is preferred.

Further, we consider models with small magnetic fields by setting an upper limit on B_x . We find that their X-ray fits are generally, and independently from values of α and \dot{C}_{irr} , worse (models SA7 and SA8). This is explained by a particular behaviour of the accretion efficiency in the case of a strong magnetic field, which makes a knee on an X-ray light curve more pronounced (compare SA1 and SA7 in Fig. 10, the left panels). The rotating magnetosphere of the neutron star adds up to the torque at the inner disc radius and enables the disc-accretion efficiency to have a maximum when $R_{\text{in}} = R_{\text{cor}}$ (see (8), (21), and Fig. 8, the left panel, the blue dashed line).

4.5 Is there a disc at the end?

There is a possibility that a ‘left-over’ disc remains after an outburst (indicated, for example, by an observed double burst from ms pulsar IGR J00291+5934, see Hartman et al. 2011). The two flares of the pulsar separated by mere 30 days forced the authors to conclude that much of the disc was conserved after the 1st burst, apparently because the mass loss virtually stopped. This case can be calculated in the POSA or SA scenario with a pre-set value of the final disc radius R_{dead} . A final inner torque value F_{dead} is related to this radius via (12). When, in the course of viscous evolution, the torque values at the inner radii level with F_{dead} , the accretion flow through the inner edge stops. Then the emitted energy is provided by a constant inner torque F_{in} even when the accretion rate \dot{M}_{in} is zero (see Eq. (20)). A dead disc around a magnetized star produces a constant level of radiation supplied by the energy of the neutron star rotation; the flux depends on R_{dead} and B_x . For example, if we set $R_{\text{dead}} = R_{\text{cor}}$ in a model with $B_x > 10^8$ G, we get a very luminous plateau contradicting observations (see Fig. 11, the top curve). Let us consider other possibilities.

(a) A dead disc hovering at the corotation radius. $R_{\text{dead}} = R_{\text{cor}}$ and $B_x \sim (3 - 4) \times 10^7$ G, model SA11.

A scenario of a dead disc or disc-reservoir extending down to the corotation radius has a long history. It partly bases on the reasoning that the propeller mechanism cannot launch matter near the corotation radius because this is not energetically self-consistent. In a numerical time-dependent model for a disc in a binary system, Armitage & Clarke (1996) set the inner radius at R_{cor} and observe it to remain there for a long time, even when $\dot{M} = 0$, since the mass cannot

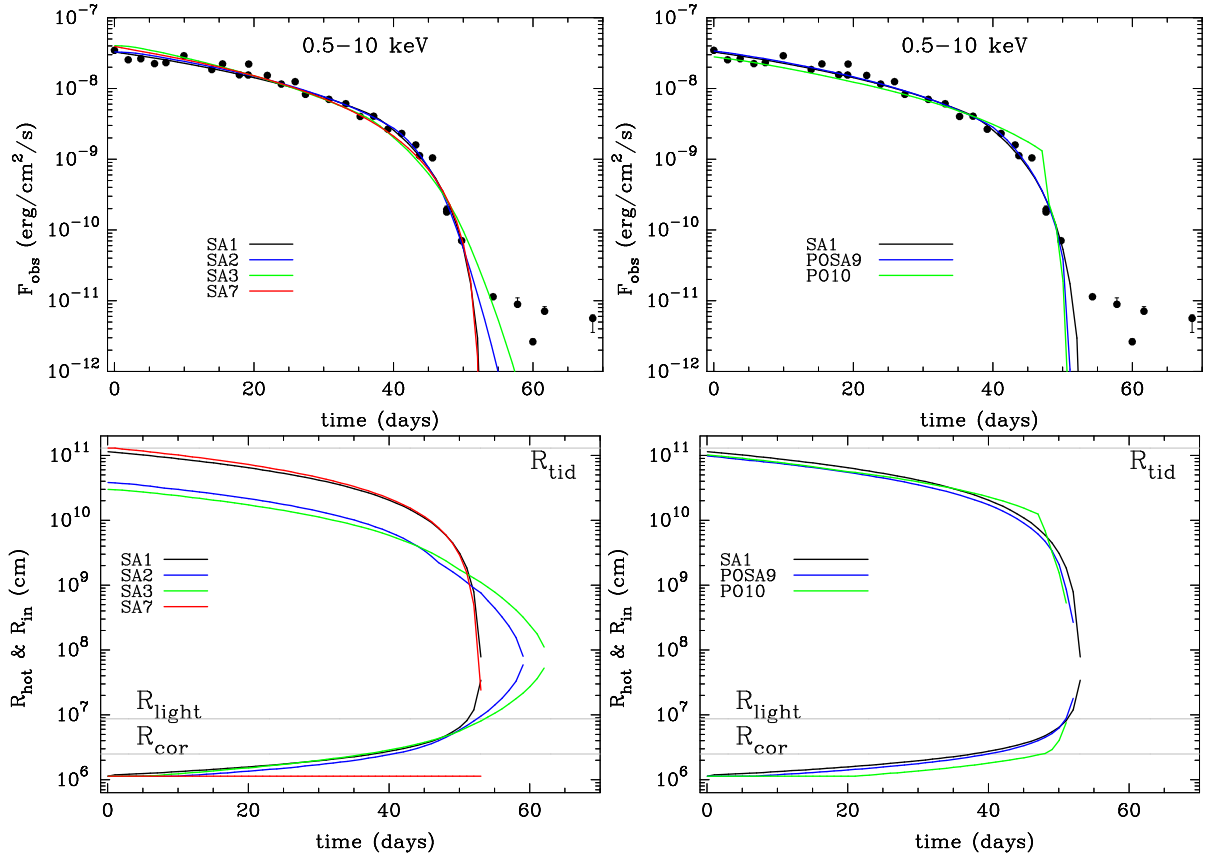


Figure 10. Comparison of different scenarios. Left: Effect of self-irradiation. Models SA2 and SA3 have C_{irr} about an order less than SA1 and SA7 do. Right: Effect of different outflow prescriptions listed in Table 1. Top: X-ray light curves. Bottom: the disc inner and hot-zone radii. The horizontal lines are, from the highest to the lowest: the tidal, the light-cylinder, and the corotation radius.

leave the disc. Rappaport et al. (2004) suggest a disc inner edge remains at the corotation radius with a decaying mass flux in order to explain high spin-down rates and apparent accretion over wide range of \dot{M} in millisecond AXPs. D’Angelo & Spruit (2012) suggest that a ‘trapped’ state of the disc is possible when the disc with an arbitrary low accretion rate ‘hovers’ around the corotation radius.

In order for the thin disc to emit not too much X-rays when its inner edge is at the corotation radius (about 15 km above the neutron star surface), the magnetic field should be lowered. In Fig. 11 we present a corresponding fit SA11. The magnetic field, consistent with such disc luminosity, i.e. to fit the plato, is a decade less than in our reference model, just $\sim (3 - 4) \times 10^7$ G.

No matter is propelled away during an outburst in such scenario and the disc’s inner radius first approaches, then oscillates around, and, finally, freezes at the corotation radius. (Though presumed, oscillations of the inner radius are not resolved in our numerical model.) It is inevitable that matter should somehow leave the disc through its inner radius until a constant F -profile settles on over the entire hot disc because the outer hot disc radius $R_{\text{hot}}(t)$ is not increasing (on the contrary, $R_{\text{hot}}(t)$ can only move inward after the peak of an outburst).

In this model, the drop of luminosity at ~ 45 th day happens due to the fast shrinking of the hot zone. We note the modeled light curve fits the X-ray data worse than the models with higher magnetic field do. However, given the schematic nature of all scenarios, this one cannot be excluded.

(b) A dead disc hovering farther than the corotation radius. $R_{\text{dead}} > R_{\text{cor}}$ and $B_x < 7.5 \times 10^8$ G, model SA12.

To match the luminosity level at the plato stage, see (7) and (20),

$$L_{\text{plato}} = \kappa_{\text{td}} \frac{\mu^2 \sqrt{G M_{\star}}}{R_{\text{dead}}^{9/2}},$$

the inner radius of the thin dead disc should be equal to $R_{\text{dead}} = R_{\text{cor}} \times (2 L_{\text{knee}}/3 L_{\text{plato}})^{2/9}$, where luminosity is bolometric. The magnetic field as in the model SA1 requires $R_{\text{dead}} \sim 3 R_{\text{cor}}$ for this to happen (model SA12, see Fig. 11). Notice that the inner radius is self-consistently less than the light cylinder radius (see Table 2): in the opposite case an accretion flow would be swept away by the pulsar wind. That is, in order for this scenario to be feasible at all, the required magnetic field cannot be too high: $B_x \lesssim 6.3 \times 10^7 \kappa_{\text{td}}^{-1/2} L_{34}^{1/2} P_{-3}^{9/4} M_{1.4}^{-1/4} R_6^{-3}$ G. For our parameters (Table 2) and estimated luminosity (§5.2), if B_x was $\gtrsim 7.5 \times 10^8$ G, the radius R_{dead} should be higher than R_{light} to comply with the plato level.

Finally, the maximum temperature in the disc, both in SA11 and SA12, is consistent with the black-body temperature obtained from the spectral fits (Fig. 11). One could not expect much accuracy here, since the disc spectrum is different from that of a black body.

4.6 The shrinking hot disc is reprocessing X-rays

We obtain that the brightness in the optical bands during the 2013 outburst of Aql X-1 can be explained only if the disc zones, emitting in

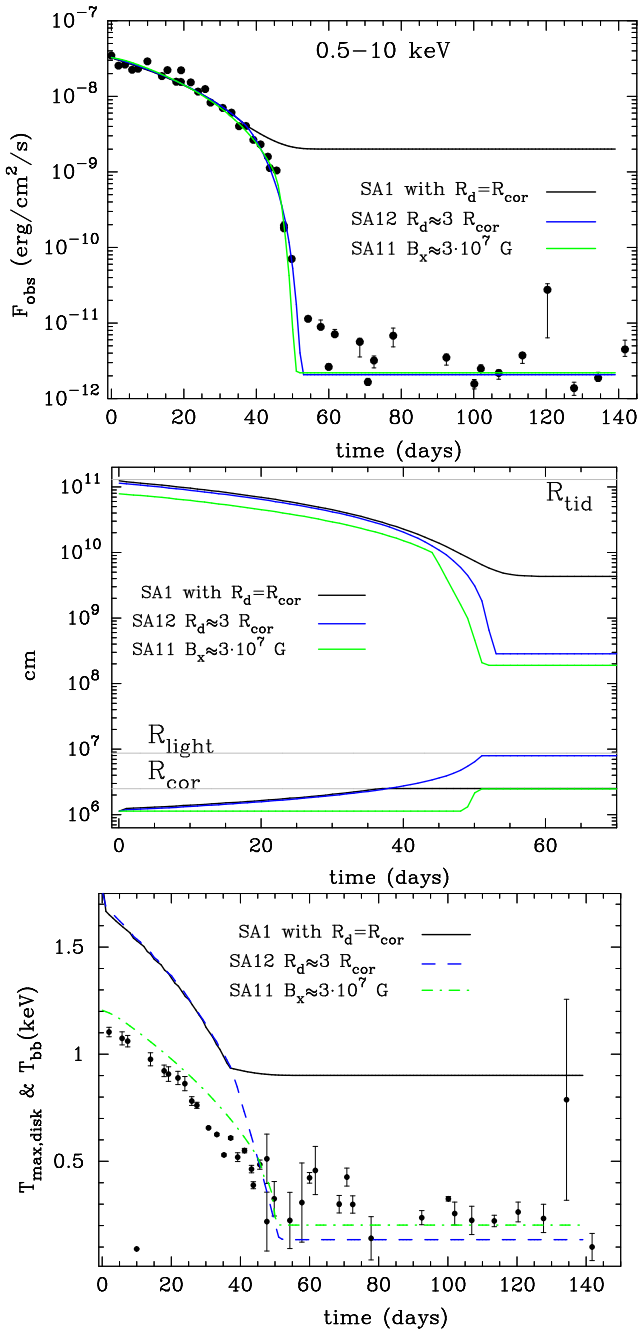


Figure 11. The models with the inner disc radius kept constant when reaching a set value. Two upper panels are similar to Fig. 10. The lower panel shows the maximum effective temperature of the disc (curves) and the black-body temperature T_{bb} from the spectral fits (dots; see §3.1).

the optical, are heated by the central X-rays. This is in agreement with the conclusion by Meshcheryakov et al. (2018) who investigated the rise of X-ray and optical light curves of the same outburst of Aql X-1 and obtained following accretion disc parameters around the outburst maximum: the disc accretion rate $\dot{M} \approx 0.66 \times \dot{M}_{\text{Edd}} = 1.29 \times 10^{18}$ g/s; the outer disc radius $R_d \approx R_{\text{tid}} = 1.9 \times R_{\odot} = 1.3 \times 10^{11}$ cm; and the irradiation parameter (responsible for all optical flux) with respect to 0.5–100 keV flux $C_{\text{irr}} \approx 10^{-3}$. The peak accretion rate \dot{M}_{in} obtained in our models with a small magnetic field (for example, SA7) agrees well with the above value from Meshcheryakov et al. (2018) (see

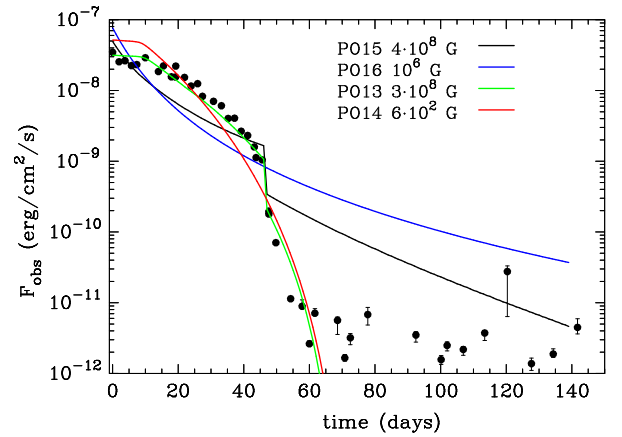


Figure 12. X-ray light curves resulted in the models without irradiation of the disc (rejected models).

Table 3). Our irradiation parameter C_{irr} agrees with the previous estimate too: it lies in the interval $(2 - 3.2) \times 10^{-3}$, see Fig. 9.

Importance of irradiation and hot-disc size change can be illustrated by a set of unsuccessful models: PO13 and below in Table 3. Supplement Figures SF?? and SF?? show the light curves obtained when the disc is non-irradiated (models PO13 and PO14, respectively). Accretion rate evolution in models with a constant-size hot zone (models PO15–PO19 in Table 3), fails to explain the X-ray light curve (see Figure 12 and supplement Figs. SF??–SF??)¹³. Thus, the ‘exponential’ stage of the disc evolution in the 2013 burst of Aql X-1 did not occur or was very short.

5 DISCUSSION

5.1 Comparison to other models

The disc viscous evolution around magnetized stars drew attention of many researchers. Evolution of a disc at the brink of the two regimes, accretion and propeller, was studied by Spruit & Taam (1993). They set a constant inflow accretion rate and considered oscillations of the disc structure when its inner radius was shifting around R_{cor} . They have set a special boundary value on the viscous torque, increasing it with increasing ω_s and representing a ‘centrifugal barrier’ of an exponential form for $\omega_s > 1$. This disc with such inner conditions is realized in our code by setting the final inner radius of the disc $R_{\text{dead}} = R_{\text{cor}}$. Oscillations of the inner edge are not resolved in our code, because it is focused on the global viscous evolution.

D’Angelo & Spruit (2010) show that if the accretion rate is slightly less than some critical accretion rate, the time scale of the oscillations is of order of the viscous time scale calculated at R_{cor} , and the oscillations look like sinusoidal modulations. The less the incoming accretion rate, the less frequently occur the ‘overflows’. D’Angelo & Spruit (2010) suggest that 1-Hz QPO demonstrated in the decline phase by the AXMP SAX J1808.8-3658 in several outbursts (Patruno et al. 2009), and by the AXMP NGC 6440 X-2, are manifestations of such oscillations near the corotation radius. There is also a 0.5 Hz QPO seen in AMXP IGR J00291+5934 (Hartman et al. 2011). D’Angelo & Spruit (2010) conclude that oscillations can continue for any low value of the accretion rate.

¹³ We choose PO scenario here because, among all scenarios, it produces steeper drops of the flux near the knee.

It is possible that during the decay of an outburst the inner disc radius, when reaching the corotation radius, continues to recede farther in an oscillatory manner. Such character of the flow was also demonstrated in numerical simulations (see references in §2). However, in an evolving disc the mass inflow decays since the mass of the hot disc diminishes. As a terminal state, the torque value at the inner edge of the disc becomes equal to the torque value at the outer edge of the hot disc: a truly ‘dead’ disc configuration emerges (Lipunova 2015). There is no movement of matter along the radius. The accretion rate is zero but the disc radiates the energy supplied by the neutron star’s spin-down, in accordance with Eq. (20) (see also §5.2).

Armitage & Clarke (1996) witnessed a formation of a disc-reservoir, limited by R_{cor} and R_{tid} , which decelerated the central star by transferring the angular momentum to the orbital motion. In their time-dependent code for a disc around a magnetized T Tauri star, they forbid accretion for $R_{\text{in}} > R_{\text{cor}}$. The outer boundary condition for their disc in a binary was the same as ours: a zero radial velocity; the mass of the disc was set as an initial condition and the inner disc edge was set just beyond R_{cor} . Differently from us they set the inner boundary condition $\Sigma = 0$ at R_{cor} and considered the magnetic torque that was distributed over radius. They have demonstrated an enhanced disc luminosity in a presence of the magnetic torque, which our model visibly reproduces.

Previously, it has been suggested that the knee position can be used to estimate the magnetic field strength of the star. It can be done if one assumes a very efficient blockage of accretion onto a star, like in our scenario PO. Equating $R_{\text{cor}} = \xi_{\text{mag}} R_{\text{mag}}$, using definitions (4) and (6), one gets

$$B_x \approx 4.3 \times 10^7 \xi_{\text{mag}}^{-7/4} \eta_{0.2}^{-1/2} L_{36}^{1/2} P_{-3}^{7/6} M_{1.4}^{5/6} R_6^{-3} \text{ G}$$

or $B_x \approx 3.6 \times 10^8 \text{ G}$ for $\xi_{\text{mag}} = 0.5$, $\eta = 0.2$, $L_{36} = 3$ (as in PO10), $P = 1/550 \text{ s}$ and $R_6 = 1.12$. This value of the magnetic field is somewhat larger than it was estimated in other works. For example, Zhang et al. (1998a) estimated the magnetic field of the neutron star as $\sim 1 \times 10^8 \text{ G}$ from the spectral analysis of 1997 outburst. The difference is caused by the distance they assumed (2.5 kpc; this explains factor of 2 since $B_x \propto L_x^{1/2}$) and their coefficient parametrizing inner radius corresponds to $\xi_{\text{mag}} \sim 1$:

Similarly, Asai et al. (2013) and Campana et al. (2014) suggested that the X-ray evolution during Aql X-1 outbursts of 1997 and 2010 demonstrated shut-off of the accretion process on to the neutron star surface due to the propeller effect. Asai et al. (2013) estimated the magnetic field as $(0.6 - 1.9) \times 10^8 \text{ G}$ analysing three outbursts from Aql X-1 from August 2009 to September 2012. The knee bolometric luminosity in our model PO10 is ~ 3 times more than they have estimated (partly because of the distance factor 2) and this explains our higher magnetic field estimate. For the outbursts of 1997 and 2010, Campana et al. (2014) estimated the critical luminosity as $(5 - 6) \times 10^{36} \text{ erg/s}$ and the magnetic field as $(1 - 4) \times 10^8 \text{ G}$ for the distance 4.5 kpc. Evidently, the crucial limitations to such estimates of the magnetic field are a rather uncertain factor ξ_{mag} and details of the spectral modeling, which is rather simple in our study. Moreover, if the accretion inhibition works gradually, such estimates are biased even more.

The concept of the disc evolution utilized in the present study has much similarity to a model suggested by Hartman et al. (2011). They considered the double-flare of accretion-powered millisecond pulsar IGR J00291+5934 in 2008 and came to a conclusion that (i) the disc had a shrinking zone of high viscosity; (ii) a knee on the light curves was likely to be due to the accretion inhibition by a propeller effect. We find that the X-ray evolution of Aql X-1 in 2013 can be explained

satisfactorily by the change of the hot zone size, but the additional increase in the accretion efficiency when the disc edge is around R_{cor} makes the knee more pronounced.

5.2 Persistent emission in the low state

The X-ray plato flux $2 \times 10^{-12} \text{ erg/cm}^2/\text{s}$ obtained from the spectral modeling (Fig. 11) translates into $6 \times 10^{33} \text{ erg/s}$ in 0.5 – 10 keV for isotropic radiation and 5 kpc. Assuming a non-isotropic disc-like angular distribution of emission, one obtains $4 \times 10^{33} \text{ erg/s}$ in the same spectral band (models SA11 and SA12). Corresponding bolometric luminosities of the disc are $(1 - 2) \times 10^{34} \text{ erg/s}$ (the interval appears due to different maximum temperature of the dead disc in SA11 and SA12). Important to notice that the blackbody temperature of the neutron star surface would be about 0.2 keV, consistent with observed estimates (see Fig. 11).

If one explained the bolometric luminosity $1 \times 10^{34} \text{ erg/s}$ by the accretion onto the neutron star surface, that would demand the accretion rate $5.4 \times 10^{13} \text{ g/s}$ or $8.5 \times 10^{-13} M_{\odot}/\text{yr}$. This is much less than the transfer rate $\sim 2 \times 10^{-10} M_{\odot}/\text{year}$ suggested by Shahbaz et al. (1998) in the framework of the DIM (see also refs. therein). There are two possibilities: the matter falls on the neutron star, but the rate is somehow restricted (while most matter is accumulated in the outer disc); or it is not the accretion onto the neutron star surface that produces the radiation.

The model related to the first option is proposed by Zhang et al. (1998a); Shahbaz et al. (1998); Menou et al. (1999b), according to which the thin disc is substituted by an ADAF when the accretion rate is low, and the quasi-spherical flow overcomes the centrifugal barrier (if there is one, depending on the neutron star magnetic field strength), falls onto the neutron star, and gives rise to the soft X-ray emission.

The X-ray radiation, seen at the plato, can be generated by the neutron star itself. A popular concept is that a cooling of an accretion-heated neutron star crust provides quiescent emission (Brown et al. 1998; Wijnands et al. 2017). X-ray radiation can also be produced far from the neutron star. Cui (1997) suggested for normal pulsars that X-ray emission in the low state is generated by relativistic particles accelerated in a shock produced by the propeller wind colliding with the companion star wind. When the stop radius for incoming matter is larger than the light cylinder, the pulsar relativistic wind interacts with the matter inflowing through the Roche lobe, possibly giving rise to an X-ray emitting intrabinary shock (see, e.g., Campana et al. 1998; Bogdanov et al. 2011; Wadiasingh et al. 2018).

We have considered an option that the radiation is produced mostly by the inner remnant disc in scenarios SA11 and SA12. In such a case, the X-ray plato slow evolution is determined by the hot disc size evolution, which, in turn, is governed by the matter flow across the boundary between the hot and cold part of the disc.

5.3 What makes different bursts: irradiation and peak accretion rate

Using our code, we can generate a family of light curves of a source, varying only the peak accretion rate. Figure 13 shows such X-ray light curves for the same parameters as we use for Aql X-1. All curves, except one, have the same α and C_{irr} (see the caption). The lowest curve is calculated for a smaller value of C_{irr} ; subsequently, the radius of the hot disc is smaller, and the evolution is faster.

The lower panel of Fig. 13 presents a family of light curves of an X-ray transient with a negligible magnetic field of neutron star

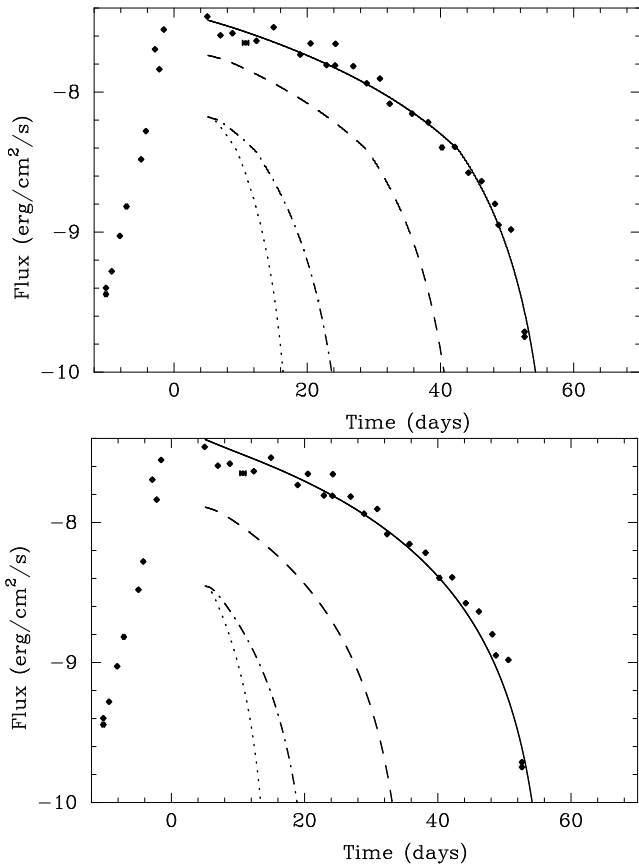


Figure 13. Upper panel: Modeled light curves with different peak accretion rates \dot{M}_0 (7.3×10^{17} , 3.5×10^{17} , and 1×10^{17} g/s), $B_x \approx 6.3 \times 10^8$ G, $\alpha = 0.74$, and $\tilde{C}_{\text{irr}} = 0.0014$. The lowest dotted model curve with faster decay has $\tilde{C}_{\text{irr}} = 0.0007$. The 2013 outburst is shown with dots. In the lower panel the light curves are calculated for the same disc parameters, except that $\dot{M}_0 = 1.1 \times 10^{18}$, 3.5×10^{17} , and 1×10^{17} g/s and the magnetic field $B_x = 100$ G.

and a shrinking hot zone. The fast evolution can be seen, although a characteristic knee is smoothed out. The knee is more pronounced in the models with high magnetic field because the accretion efficiency in the disc varies non-monotonically (see Fig. 8, the blue dashed line). When the magnetic field is low, the accretion rate efficiency is constant (see model SA7 in Supplement Material). Less width of outbursts is explained by smaller hot zones due to lower X-ray emission that lacks the energy gained from the rotation of a fast-rotating magnetized neutron star (cf. Eq.20). Its contribution is most notable when the inner disc radius approaches the corotation radius.

6 SUMMARY

A model and a computer code `FREDDI` are presented to calculate viscous disc evolution in an X-ray transient with an accreting magnetized neutron star. The accretion rate evolution is obtained by solving the viscous evolution equation for an α -disc, with no *ad hoc* time dependences. The key parameters of the model are the mass, spin frequency, and magnetic field of the accretor, the α -parameter and the degree of self-irradiation of the disc. Light curves produced by thermal radiation can be calculated with `FREDDI`.

Specific boundary conditions are set in order to input essential physics of the disc-magnetosphere interactions. Our method uses an

inference that viscous and magnetohydrodynamic processes at the disc inner boundary, being relatively fast on a whole-disc timescale, can be time-averaged and approximated by smooth conditions when solving the equation of the disc evolution.

Three scenarios of centrifugal inhibition of accretion on a neutron star are included so far: ‘instant’ block of accretion and effective propeller outflow from the corotation radius (PO), MHD-calculations-based gradual blocking and propelling with continued star accretion (POSA), and no mass propelling (SA).

We apply our model to an outburst of Aql X-1. This source and this particular outburst of 2013 have got a wealth of observational data in different spectral bands. The model is successful at explaining the X-ray and optical evolution, including a characteristic fast drop of the X-ray light curve.

The irradiation of the disc plays a major role in the evolution of the outburst of Aql X-1. In particular, the characteristic bend (a ‘knee’) of the X-ray light curve is explained by the viscous evolution of the hot zone with time-dependent outer radius determined by the condition of the irradiation temperature, $T_{\text{irr}} = 10^4$ K. Resulting parameter α is positively correlated with the irradiation parameter \tilde{C}_{irr} . This is due to the fact that increasing turbulent parameter α (or kinematic coefficient of viscosity ν_t) accelerates the mass-accretion evolution, and increasing the irradiation parameter \tilde{C}_{irr} (or the size of the ionized disc) decelerates the evolution since characteristic time $\propto R_{\text{hot}}^2/\nu_t$. In the best models the hot part of the disc (where $T_{\text{irr}} > 10^4$ K) can extend to the radius $0.85 - 0.95$ of $\sim R_{\text{tid}}$ at the peak of the outburst. This radius correlates with the irradiation parameter, which is estimated as $C_{\text{irr}}^{\text{max}} = (1.4 - 2.8) \cdot 10^{-3}$ for $\alpha = 0.5 - 0.8$.

A variation of C_{irr} with time is strongly favoured in the model to satisfactorily explain the form of the X-ray light curve. This is consistent with being the geometry effect.

Assessment of α requires a satisfactory fit to optical, which is hampered by uncertainties of the distance to the source, optical star temperature, etc. For the parameters assumed, the optical flux is explained by the irradiation of the disc with the geometrical size close to the tidal radius $\sim R_{\text{tid}}$ with a contribution from the optical companion. A scatter of the optical data indicate that reprocessing of X-rays occurs with an orbit- or near-orbital modulation, superimposed on the X-ray variations, seen on a scale of days. We find that the optical data scatter is comparable with the oscillations produced by the optical companion with albedo $\gtrsim 0.5$. Ignoring optical contribution the cold disc and optical companion results in a larger hot disc, which naturally affects the rate of the viscous evolution, requiring larger α .

We find that the light curve of Aql X-1 (2013) can be tolerably approximated without invoking the magnetosphere action (with coefficient of determination $\mathcal{R}^2 \approx 0.98$). At the same time, models with magnetic field $> 10^8$ G are statistically preferred (χ^2 is 1.5 times less) because they produce a more pronounced knee on a light curve due to the accretion-efficiency dependence on the inner disc radius. For high magnetic fields, $> 10^8$ G, we find that the X-ray data favors the scenarios with gradual extinction of matter flow to the neutron star surface. Scenario PO with an abrupt block of accretion flow at the centrifugal barrier does twice as worse comparing to scenarios with a continued accretion through the magnetospheric boundary. Resulting values of the magnetic field are $(5 - 9) \cdot 10^8$ G for SA and POSA scenarios and $(3 - 4) \cdot 10^8$ G, for the PO scenario. These values depend strongly on the definition of the magnetospheric radius (4) and distance to the source.

We also find an interesting possibility that the X-ray plateau is produced by a remnant disc-reservoir with stalled accretion. This is possible if the magnetic field is in the range $3 \times 10^7 - 6 \times 10^8$ G

(for distance 5 kpc). The temperature 0.2 – 0.3 keV of the blackbody component in the X-ray ‘blackbody plus power-law tail’ spectrum of Aql X-1 in 2013 is about the maximum temperature of that disc-reservoir.

ACKNOWLEDGMENTS

The authors are grateful to the anonymous referee for extensive helpful suggestions and to Alexander Meshcheryakov for the fruitful discussions. This work is supported by the Russian Science Foundation grant 21-12-00141 and performed in Moscow Lomonosov State University (theoretical model development and model analysis of the Aql X-1 2013 outburst). Optical data processing was supported by the grant 14.W03.31.0021 of the Ministry of Science and Higher Education of the Russian Federation and the grant from Academy of Finland 332666. X-ray data spectral modeling was supported by the Interdisciplinary Scientific and Educational School of Moscow University "Fundamental and Applied Space Research". This research has made use of data obtained through the High Energy Astrophysics Science Archive Research Center Online Service, provided by the NASA/Goddard Space Flight Center. This research has made use of the NASA/IPAC Infrared Science Archive, which is funded by the National Aeronautics and Space Administration and operated by the California Institute of Technology. This work made use of data supplied by the UK Swift Science Data Centre at the University of Leicester. This paper has made use of the SMARTS optical/near-infrared light curves. The Yale SMARTS XRB team is supported by NSF grants 0407063 and 070707. This research has made use of NASA’s Astrophysics Data System Bibliographic Services.

DATA AVAILABILITY

Authors intend to make available unabsorbed X-ray flux in 0.5-10 keV and optical flux density data of Aql X-1 used for fitting at VizierR database of astronomical catalogues. Code FREDDI can be found at <https://ascl.net/1610.014>.

REFERENCES

Alpar M. A., 2001, *ApJ*, 554, 1245
 Aly J. J., 1980, *A&A*, 86, 192
 Antokhina E. A., 1988, *Soviet Ast.*, 32, 608
 Armitage P. J., Clarke C. J., 1996, *MNRAS*, 280, 458
 Asai K., et al., 2013, *ApJ*, 773, 117
 Bagińska P., Różańska A., Czerny B., Janiuk A., 2021, *ApJ*, 912, 110
 Balbus S. A., Mummery A., 2018, *MNRAS*, 481, 3348
 Basko M. M., Sunyaev R. A., Titarchuk L. G., 1974, *A&A*, 31, 249
 Bell K. R., Lin D. N. C., 1994, *ApJ*, 427, 987
 Bessolaz N., Zanni C., Ferreira J., Keppens R., Bouvier J., 2008, *A&A*, 478, 155
 Bogdanov S., Archibald A. M., Hessels J. W. T., Kaspi V. M., Lorimer D., McLaughlin M. A., Ransom S. M., Stairs I. H., 2011, *ApJ*, 742, 97
 Bohlin R. C., Savage B. D., Drake J. F., 1978, *ApJ*, 224, 132
 Brown E. F., Bildsten L., Rutledge R. E., 1998, *ApJ*, 504, L95
 Buxton M. M., Bailyn C. D., Capelo H. L., Chatterjee R., Dinçer T., Kalemci E., Tomsick J. A., 2012, *AJ*, 143, 130
 Campana S., Stella L., Mereghetti S., Colpi M., Tavani M., Ricci D., Dal Fiume D., Belloni T., 1998, *ApJ*, 499, L65
 Campana S., Coti Zelati F., D’Avanzo P., 2013, *MNRAS*, 432, 1695
 Campana S., Brivio F., Degenaar N., Mereghetti S., Wijnands R., D’Avanzo P., Israel G. L., Stella L., 2014, *MNRAS*, 441, 1984

Casella P., Altamirano D., Patruno A., Wijnands R., van der Klis M., 2008, *ApJ*, 674, L41
 Chashkina A., Abolmasov P., Poutanen J., 2017, *MNRAS*, 470, 2799
 Cui W., 1997, *ApJ*, 482, L163
 D’Angelo C. R., Spruit H. C., 2010, *MNRAS*, 406, 1208
 D’Angelo C. R., Spruit H. C., 2012, *MNRAS*, 420, 416
 Davidson K., Ostriker J. P., 1973, *ApJ*, 179, 585
 Davis S. W., Blaes O. M., Hubeny I., Turner N. J., 2005, *ApJ*, 621, 372
 Dubus G., Lasota J.-P., Hameury J.-M., Charles P., 1999, *MNRAS*, 303, 139
 Dubus G., Hameury J.-M., Lasota J.-P., 2001, *A&A*, 373, 251
 Ekşi K. Y., 2012, arXiv e-prints, p. arXiv:1210.5330
 Elsner R. F., Lamb F. K., 1977, *ApJ*, 215, 897
 Ertan Ü., 2017, *MNRAS*, 466, 175
 Ertan Ü., 2018, *MNRAS*, 479, L12
 Evans P. A., et al., 2007, *A&A*, 469, 379
 Evans P. A., et al., 2009, *MNRAS*, 397, 1177
 Fürst F., et al., 2017, *A&A*, 606, A89
 Galloway D. K., Muno M. P., Hartman J. M., Psaltis D., Chakrabarty D., 2008, *ApJS*, 179, 360
 Ghosh P., Lamb F. K., 1979, *ApJ*, 234, 296
 Ghosh P., Pethick C. J., Lamb F. K., 1977, *ApJ*, 217, 578
 Gilfanov M., Revnivtsev M., Sunyaev R., Churazov E., 1998, *A&A*, 338, L83
 Green G. M., Schlafly E., Zucker C., Speagle J. S., Finkbeiner D., 2019, *ApJ*, 887, 93
 Güngör C., Güver T., Ekşi K. Y., 2014, *MNRAS*, 439, 2717
 Güngör C., Ekşi K. Y., Göğüş E., Güver T., 2017, *ApJ*, 848, 13
 Hameury J. M., 2020, *Advances in Space Research*, 66, 1004
 Hartman J. M., Watts A. L., Chakrabarty D., 2009, *ApJ*, 697, 2102
 Hartman J. M., Galloway D. K., Chakrabarty D., 2011, *ApJ*, 726, 26
 Illarionov A. F., Sunyaev R. A., 1975, *A&A*, 39, 185
 Illenseer T. F., Duschl W. J., 2015, *MNRAS*, 450, 691
 Ketsaris N. A., Shakura N. I., 1998, *Astronomical and Astrophysical Transactions*, 15, 193
 King A. R., Ritter H., 1998, *MNRAS*, 293, L42
 Kley W., 1991, *A&A*, 247, 95
 Kluźniak W., Rappaport S., 2007, *ApJ*, 671, 1990
 Kolesnikov D., et al., 2020, *Contributions of the Astronomical Observatory Skalnaté Pleso*, 50, 518
 Kulkarni A. K., Romanova M. M., 2013, *MNRAS*, 433, 3048
 Lamb F. K., Pethick C. J., Pines D., 1973, *ApJ*, 184, 271
 Landau L., Lifshitz E., 1976, *Mechanics*. Butterworth-Heinemann, Butterworth-Heinemann, <https://books.google.ru/books?id=e-xASAehg1sC>
 Lasota J.-P., 2001, *New Astronomy Review*, 45, 449
 Lii P. S., Romanova M. M., Ustyugova G. V., Koldoba A. V., Lovelace R. V. E., 2014, *MNRAS*, 441, 86
 Lipunov V. M., 1978, *Soviet Ast.*, 22, 702
 Lipunov V. M., 1980, *Soviet Ast.*, 24, 722
 Lipunov V. M., 1981, *Soviet Ast.*, 25, 375
 Lipunov V. M., 1982a, *Astronomy Letters*, 26, 537
 Lipunov V. M., 1982b, *Ap&SS*, 85, 451
 Lipunov V. M., 1992, *Astrophysics of Neutron Stars*. Springer-Verlag, Berlin
 Lipunova G. V., 2015, *ApJ*, 804, 87
 Lipunova G. V., Malanchev K. L., 2017, *MNRAS*, 468, 4735
 Lipunova G. V., Shakura N. I., 2000, *A&A*, 356, 363
 Lipunova G., Malanchev K., Shakura N., 2018, *The Standard Model of Disc Accretion*. p. 1, doi:10.1007/978-3-319-93009-1_1
 Long M., Romanova M. M., Lovelace R. V. E., 2005, *ApJ*, 634, 1214
 Ludwig K., Meyer-Hofmeister E., Ritter H., 1994, *A&A*, 290, 473
 Lutovinov A. A., Tsygankov S. S., Krivonos R. A., Molkov S. V., Poutanen J., 2017, *ApJ*, 834, 209
 Lynden-Bell D., Pringle J. E., 1974, *MNRAS*, 168, 603
 Lyubarskij Y. E., Shakura N. I., 1987, *Soviet Astronomy Letters*, 13, 386
 Lyutyi V. M., Sunyaev R. A., 1976, *Soviet Ast.*, 20, 290
 Malanchev K. L., Lipunova G. V., 2016, *Freddi: Fast Rise Exponential Decay accretion Disk model Implementation*; ascl:1610.014
 Malanchev K. L., Postnov K. A., Shakura N. I., 2017, *MNRAS*, 464, 410

Mata Sánchez D., Muñoz-Darias T., Casares J., Jiménez-Ibarra F., 2017, *MNRAS*, 464, L41

Matsuoka M., Asai K., 2013, *PASJ*, 65, 26

Matt S., Pudritz R. E., 2005, *MNRAS*, 356, 167

Menou K., Hameury J.-M., Stehle R., 1999a, *MNRAS*, 305, 79

Menou K., Esin A. A., Narayan R., Garcia M. R., Lasota J.-P., McClintock J. E., 1999b, *ApJ*, 520, 276

Mescheryakov A. V., Shakura N. I., Suleimanov V. F., 2011, *Astronomy Letters*, 37, 311

Mescheryakov A. V., Tsygankov S. S., Khamitov I. M., Shakura N. I., Bikmaev I. F., Eiselevich M. V., Vlasyuk V. V., Pavlinsky M. N., 2018, *MNRAS*, 473, 3987

Mushtukov A. A., Lipunova G. V., Ingram A., Tsygankov S. S., Mönkkönen J., van der Klis M., 2019, *MNRAS*, 486, 4061

Nixon C. J., Pringle J. E., 2020, arXiv e-prints, p. arXiv:2008.07565

Özel F., Freire P., 2016, *ARA&A*, 54, 401

Papaloizou J., Pringle J. E., 1977, *MNRAS*, 181, 441

Parfrey K., Tchekhovskoy A., 2017, *ApJ*, 851, L34

Parfrey K., Spitkovsky A., Beloborodov A. M., 2017, *MNRAS*, 469, 3656

Patruno A., Watts A., Klein Wolt M., Wijnand s R., van der Klis M., 2009, *ApJ*, 707, 1296

Powell C. R., Haswell C. A., Falanga M., 2007, *MNRAS*, 374, 466

Pringle J. E., 1991, *MNRAS*, 248, 754

Pringle J. E., Rees M. J., 1972, *A&A*, 21, 1

Rafikov R. R., 2016, *ApJ*, 830, 7

Raguzova N. V., Lipunov V. M., 1998, *A&A*, 340, 85

Rappaport S. A., Fregeau J. M., Spruit H., 2004, *ApJ*, 606, 436

Rodrigo C., Solano E., Bayo A., 2012, SVO Filter Profile Service Version 1.0, IVOA Working Draft 15 October 2012, doi:10.5479/ADS/bib/2012ivoa.rept.1015R

Romanova M. M., Ustyugova G. V., Koldoba A. V., Lovelace R. V. E., 2005, *ApJ*, 635, L165

Romanova M. M., Ustyugova G. V., Koldoba A. V., Lovelace R. V. E., 2009, *MNRAS*, 399, 1802

Romanova M. M., Blinova A. A., Ustyugova G. V., Koldoba A. V., Lovelace R. V. E., 2018, *New Astron.*, 62, 94

Sakurai S., Yamada S., Torii S., Noda H., Nakazawa K., Makishima K., Takahashi H., 2012, *PASJ*, 64, 72

Schlaflly E. F., Finkbeiner D. P., 2011, *ApJ*, 737, 103

Schlegel D. J., Finkbeiner D. P., Davis M., 1998, *ApJ*, 500, 525

Schultz G. V., Wiemer W., 1975, *A&A*, 43, 133

Shahbaz T., Charles P. A., King A. R., 1998, *MNRAS*, 301, 382

Shakura N. I., 1973, *Soviet Astronomy*, 16, 756

Shakura N. I., Sunyaev R. A., 1973, *A&A*, 24, 337

Shakura N. I., Sunyaev R. A., 1988, *Advances in Space Research*, 8, 135

Shimura T., Takahara F., 1995, *ApJ*, 445, 780

Shvartsman V., 1970, *Radiofizika*, 13, 1852

Smak J., 1984, *Acta Astronomica*, 34, 161

Spruit H. C., Taam R. E., 1993, *ApJ*, 402, 593

Stella L., White N. E., Rosner R., 1986, *ApJ*, 308, 669

Suleimanov V., Meyer F., Meyer-Hofmeister E., 1999, *A&A*, 350, 63

Suleimanov V. F., Lipunova G. V., Shakura N. I., 2007, *Astronomy Reports*, 51, 549

Suleimanov V. F., Lipunova G. V., Shakura N. I., 2008, *A&A*, 491, 267

Sunyaev R. A., Shakura N. I., 1977, *Pisma v Astronomicheskii Zhurnal*, 3, 262

Sunyaev R. A., Shakura N. I., 1977, *Soviet Astronomy Letters*, 3, 138

Sunyaev R. A., Shakura N. I., 1986, *Pisma v Astronomicheskii Zhurnal*, 12, 286

Taam R. E., Meszaros P., 1987, *ApJ*, 322, 329

Tanaka T., 2011, *MNRAS*, 410, 1007

Tsygankov S. S., Lutovinov A. A., Doroshenko V., Mushtukov A. A., Suleimanov V., Poutanen J., 2016, *A&A*, 593, A16

Tuchman Y., Mineshige S., Wheeler J. C., 1990, *ApJ*, 359, 164

Ustyugova G. V., Koldoba A. V., Romanova M. M., Chechetkin V. M., Lovelace R. V. E., 1999, *ApJ*, 516, 221

Ustyugova G. V., Koldoba A. V., Romanova M. M., Lovelace R. V. E., 2006, *ApJ*, 646, 304

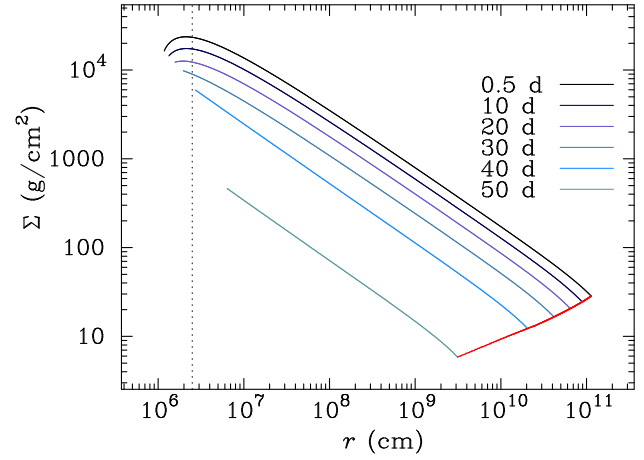


Figure A1. Surface density distributions in the ionized part of the disc in SA1 model at different times labeled from top to bottom. The vertical line marks the corotation radius.

Wadiasingh Z., Venter C., Harding A. K., Böttcher M., Kilian P., 2018, *ApJ*, 869, 120

Wang Y.-M., 1987, *A&A*, 183, 257

Wang Y.-M., 1995, *ApJ*, 449, L153

Wang Y. M., 1996, *ApJ*, 465, L111

White N. E., Zhang W., 1997, *ApJ*, 490, L87

Wijnands R., Degenaar N., Page D., 2017, *Journal of Astrophysics and Astronomy*, 38, 49

Zanni C., Ferreira J., 2013, *A&A*, 550, A99

Zhang S. N., Yu W., Zhang W., 1998a, *ApJ*, 494, L71

Zhang W., Jahoda K., Kelley R. L., Strohmayer T. E., Swank J. H., Zhang S. N., 1998b, *ApJ*, 495, L9

APPENDIX A: VERTICAL STRUCTURE

To obtain a relation between the surface density Σ and the viscous stress tensor $W_{r\phi}$, one needs to solve the vertical structure equations. In the FREDDI code, physical parameters (column density Σ , semithickness z_0 , etc.) at any radius are found using analytic approximations to numerical solutions of the disc vertical structure (Ketsaris & Shakura 1998; Malanchev et al. 2017; Lipunova et al. 2018). The surface density in the disc is as follows:

$$\Sigma \approx 34 \text{ g/cm}^2 \alpha^{-7/9} r_{10}^{-2/3} \dot{M}_{17}^{2/3} m_x^{2/9}$$

for the opacity approximation of Bell & Lin (1994), appropriate for the solar chemical abundances:

$$\kappa = \kappa_0 \frac{\rho^{\zeta}}{T^{\nu}}, \quad \zeta \approx 1, \nu \approx 5/2, \quad \kappa_0 \approx 1.5 \cdot 10^{20} \text{ cm}^5 \text{ K}^{5/2} \text{ g}^{-2}.$$

In Fig. A1, the surface density distributions are presented, corresponding to torque distributions shown in Fig. 3 in model SA1. The red line is the surface density left after the burst passed by, $\Sigma(R_{\text{hot}}(t))$. Qualitatively, this picture resembles the burst evolution obtained by Dubus et al. (2001) (see their figure 12). Corresponding disc semithickness is

$$z_0/r \approx 0.05 \alpha^{-1/9} r_{10}^{1/12} \dot{M}_{17}^{1/6} m_x^{-13/36}.$$

We note that a structure of a non-irradiated disc is used in the model with irradiation contributing significantly to the optical flux, which is justified by the previously obtained results. As suggested by Lyutyi & Sunyaev (1976) and confirmed by Mesheryakov et al. (2011), the irradiated disc in the hot zone does not change significantly its

vertical structure comparing to the case without irradiation, due to its large optical thickness (see also [Dubus et al. 1999](#)).

The region, evacuated by the hot disc when it shrinks, is likely optically-thin. In such a case, to explain the optical ‘black-body’ emission from a cold zone of size of the tidal radius $\sim R_{\text{tid}}$ we suggest that there is a ‘cold’ dense ring of non-ionised matter near R_{tid} that survives an outburst. Its temperature is very low, and we assume that it shines only by reprocessing X-rays, possibly scattered by the plasma above the disc. This ring casts a shadow on the optical companion when it is thicker than the hot disc. The optically thin matter may form a corona, similar to the Solar one, with characteristic temperatures around 10^6 K at distances $\sim 10^{11}$ cm. The characteristic time of such corona formation is $1/(\alpha \omega_K)$.

APPENDIX B: BOLOMETRIC LUMINOSITY OF THE NEUTRON STAR

The momentum equation for the matter moving in the magnetosphere yields the following energy integral ([Ghosh et al. 1977](#); [Ustyugova et al. 1999](#)):

$$\frac{1}{2} (v_p^2 + \omega^2 r^2) - \omega_\star \omega r^2 - \frac{G M_\star}{r} = \text{const},$$

where v_p is the poloidal speed and ω is the angular velocity of the matter. We assume that the poloidal speed at inner disc radius R_{in} is zero and the radiated energy results from the kinetic energy of the poloidal speed at the neutron star surface. Then, luminosity due to accretion onto a neutron star can be written as follows

$$L_\star = \frac{\dot{M}_\star G M_\star}{R_\star} \left(1 - \frac{R_\star}{R_{\text{in}}} \right) + \frac{\dot{M}_\star \omega_\star^2}{2} (R_\star^2 - R_{\text{in}}^2) + \frac{\dot{M}_\star G M_\star}{2 R_{\text{in}}} \left(1 - \frac{\omega_\star}{\omega_K(R_{\text{in}})} \right)^2. \quad (\text{B1})$$

and (22) is easily obtained. The terms in the last expression were rearranged in an attempt to associate them with specific processes during the matter motion. The first term is the work by the gravitational forces. The second term is the change of the ‘centrifugal energy’ in the co-rotating coordinate system (c.f. [Landau & Lifshitz §39, 1976](#)), or the work by electromagnetic forces in the inertial coordinate system. The third term is due to the braking of the matter angular velocity from the Keplerian $\omega_K(R_{\text{in}})$ to the magnetospheric ω_\star . This term can be compared to the heat released at the surface of a star rotating slower than an adjacent disc, which is obtained from the conservation of momentum and energy (e.g., [Shakura & Sunyaev 1988](#); [Kley 1991](#)):

$$L_\star = \frac{\dot{M} G M_\star}{2 R_\star} \left(1 - \frac{\omega_\star}{\omega_K(R_\star)} \right)^2. \quad (\text{B2})$$

When the magnetic field is not important, the orbiting matter decelerates from a Keplerian velocity to the rotational velocity on the neutron star, and the extra energy is turned into heat.

Expression (B1) applies for both the case of small and large magnetic field. It depends on the accretion rate, if there is a magnetosphere ($R_{\text{mag}} > R_\star$). Some of the kinetic energy, related to the orbital motion of the matter in the disc is spent on the neutron-star’s spin-up, and the rest energy is released as the heat on the neutron star’s surface. For high accretion rates, the disc overwhelms the magnetic field, which can be thus ignored. Then $R_{\text{mag}} = R_\star$, and only the last term survives in (B1), becoming (B2), independent from \dot{M} . If $R_{\text{mag}} = R_\star$ and the star does not rotate, it radiates the same energy as the disc.

APPENDIX C: OPTICAL EXTINCTION TOWARDS AQL X-1

IRSA Dust service¹⁴ gives colour excess in the direction of the source as $E_{B-V} = 0.61 \pm 0.02$ for COBE/DIRBE and IRAS/ISSA maps ([Schlegel et al. 1998](#)) and $E_{B-V} = 0.71 \pm 0.03$ for [Schlafly & Finkbeiner \(2011\)](#) map based on SDSS spectral data. 3D Dust Mapping service¹⁵ gives colour excess $E_{B-V} = 0.64^{+0.02}_{-0.03}$ for distance of 5 kpc ([Green et al. 2019](#)). According to these data we use $E_{B-V} = 0.64 \pm 0.04$, taking into account the uncertainty in the photometric data. We use standard relation between the colour excess and visual extinction: $A_V = 3.1 E_{B-V}$ ([Schultz & Wiemer 1975](#)).

[Sakurai et al. \(2012\)](#), performing for the Aql X-1 outburst of 2007 spectral fits in 0.5–30 keV, obtains $N_H = 3.6 \cdot 10^{21}$ atoms/cm². Taking into account $N_H/E_{B-V} = 5.8 \cdot 10^{21}$ atoms/cm²/mag ([Bohlin et al. 1978](#)) it would give $E_{B-V} = 0.62$. Our spectral modeling of the Swift/XRT data gives $N_H = (5.5 \pm 0.2) \cdot 10^{21}$ atoms/cm² (see §3.1). Thus, the values obtained from X-ray observations, agree with the above $E(B-V)$.

We transform the visual extinction to that in particular optical passbands using SVO Filter Profile Service¹⁶ ([Rodrigo et al. 2012](#)). It gives the following values for the A_f/A_V ratio: $UVW2 = 3.09$, $UVM2 = 3.02$, $UVW1 = 2.06$, $U = 1.62$, $B = 1.32$, $V = 1.02$, $R = 0.82$, and $J = 0.3$.

¹⁴ <https://irsa.ipac.caltech.edu/applications/DUST/>

¹⁵ <http://argonaut.skymaps.info/query>

¹⁶ <http://svo2.cab.inta-csic.es/theory/fps/>

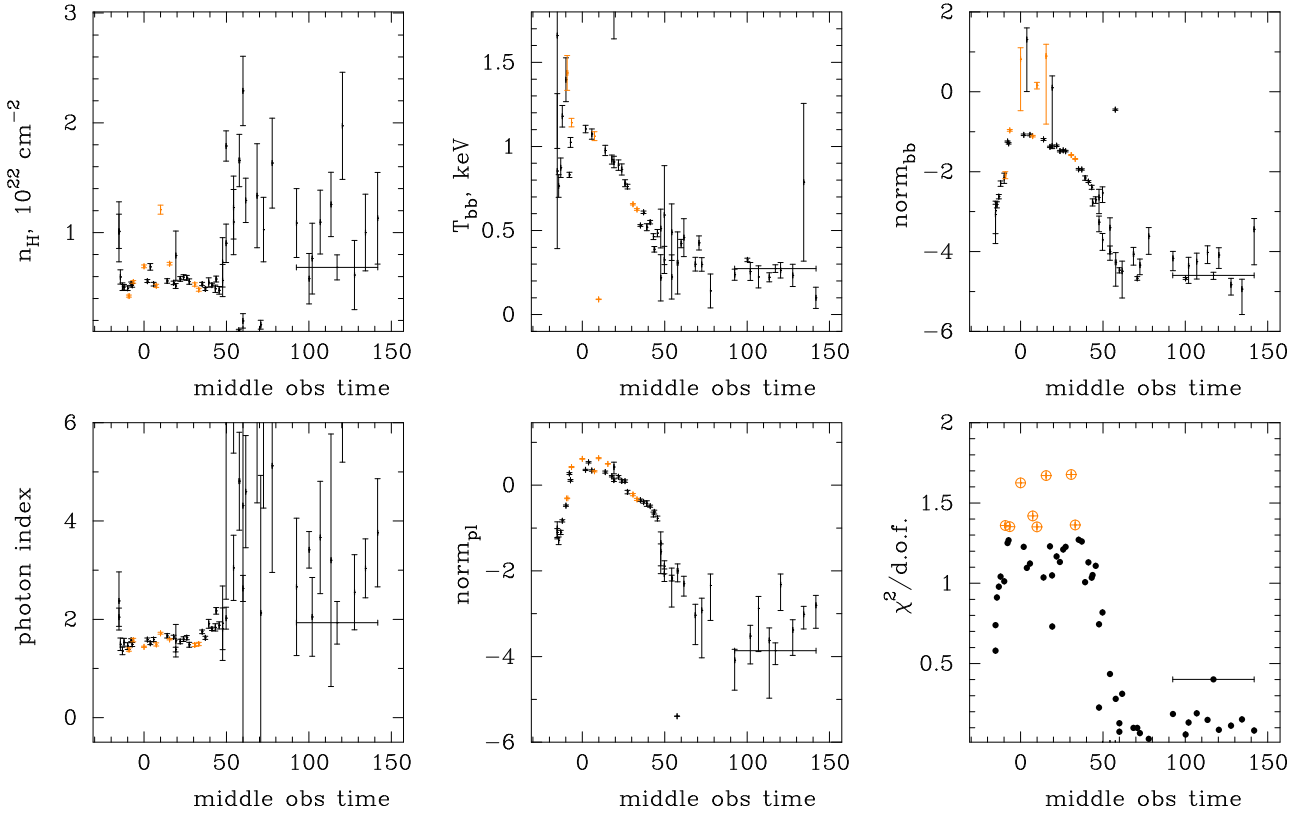


Figure A2. Evolution of the spectral parameters for model `tbabs*(bbody+powerlaw)`. Orange color indicate fits with reduced $\chi^2 > 1.3$. Zero time is MJD 56466.763. The point with the long horizontal bar is derived from the spectrum integrated over MJD 56550-56650 and used for fits SA11 and SA12.